Acta Pharmaceutica Sinica B 2026;16(1):252−269

Chinese Pharmaceutical Association
Institute of Materia Medica, Chinese Academy of Medical Sciences

Acta Pharmaceutica Sinica B

www.elsevier.com/locate/apsb
www.sciencedirect.com

ORIGINAL ARTICLE

Radiation-induced nuclear translocation of NPRL2 hijacks E3 ubiquitin ligases to enhance DNA repair *via* the AMPK/WDR24 axis, contributing to CRC radioresistance

Xuecen Wang[a,†], Yuxuan Zhao[b,†], Xingli Yang[a,†], Tingyu Liu[c,†], Weilin Zhou[b], Shaoqing Niu[a], Meng Jin[d], Yong Chen[a], Ran-yi Liu[c,*], Yong Bao[a,*], Xin Yue[b,*]

[a]*Department of Radiation Oncology, The First Affiliated Hospital, Sun Yat-sen University, Guangzhou 510080, China*
[b]*State Key Laboratory of Bioactive Molecules and Druggability Assessment, The First Affiliated Hospital of Jinan University, Guangzhou, Guangdong 510630, China*
[c]*State Key Laboratory of Oncology in South China, Sun Yat-sen University Cancer Center, Guangzhou 510060, China*
[d]*Department of Radiation Oncology and Jilin Provincial Key Laboratory of Radiation Oncology & Therapy, The First Hospital of Jilin University, Changchun 130021, China*

Received 10 April 2025; received in revised form 13 August 2025; accepted 9 September 2025

KEY WORDS

NPRL2;
Nuclear translocation;
Radiation induction;
E3 ubiquitin ligases;
DNA repair;
AMPK/WDR24 axis;
CRC radioresistance;
Therapeutic target

Abstract Radiotherapy resistance remains a major clinical challenge in colorectal cancer (CRC) treatment. Our study reveals that the regulation of nuclear E3 ubiquitin ligase maintains K48-ubiquitin levels that correlate with CRC radiotherapy sensitivity. We identify NPRL2 as the central mediator of this process. Following radiation, NPRL2 rapidly translocates to the nucleus, where it directly binds to the catalytic domains of key E3 ubiquitin ligases, including HERC2 and RNF8, and functionally inactivates them. This NPRL2-mediated inhibition of E3 ligase activity prevents the degradation of critical DNA repair proteins. Importantly, clinical analyses demonstrate that nuclear NPRL2 plays a role in sustaining radioresistance. Mechanistic investigations reveal that radiation-induced AMPK activation initiates this process by phosphorylating WDR24, which promotes NPRL2 dissociation from the GATOR1 complex and facilitates its nuclear translocation. Therapeutic targeting through AMPK inhibition effectively

*Corresponding authors.
E-mail addresses: yuex2504@jnu.edu.cn (Xin Yue), baoyong@mail.sysu.edu.cn (Yong Bao), liury@sysucc.org.cn (Ran-yi Liu).
[†]These authors made equal contributions to this work.

Peer review under the responsibility of Chinese Pharmaceutical Association and Institute of Materia Medica, Chinese Academy of Medical Sciences.

https://doi.org/10.1016/j.apsb.2025.10.039

blocks NPRL2 nuclear accumulation, leading to impaired DNA damage repair and significant radiosensitization of CRC cells in both *in vitro* and *in vivo* models. These findings not only elucidate the AMPK/WDR24/NPRL2 signaling axis as a fundamental regulator of DNA repair machinery in CRC, but also provide compelling evidence for its potential as a novel therapeutic target to overcome radioresistance and improve radiotherapy efficacy in CRC patients.

1. Introduction

Comprehensive treatment based on radiotherapy, driven by continuous technological advancements, is increasing and has been the major treatment strategy for colorectal cancer (CRC), especially for locally advanced rectal cancer (LARC)[1,2]. In recent years, the radiotherapy resistance of tumor cells has emerged as a major factor limiting the efficacy of radiotherapy and presenting a significant challenge to its wider clinical application. To better understand the mechanisms of radioresistance and develop targeted strategies to enhance radiosensitivity, it is essential to explore the molecular mechanisms underlying the response to radiation. The primary biological effect of radiation is the induction of DNA double-strand breaks (DSBs) in tumor cells, which constitutes a severe threat to genomic integrity[3]. In response to this damage, cells activate robust stress response mechanisms to rapidly repair DNA and maintain critical processes such as cell growth and metabolism. Among the various DNA repair pathways, homologous recombination (HR) and nonhomologous end joining (NHEJ) are the two primary mechanisms responsible for repairing DSBs[4,5]. By focusing on these pathways, we aim to gain a deeper understanding of the DNA repair processes involved in radiotherapy resistance and develop innovative strategies to enhance the therapeutic efficacy of radiotherapy in CRC.

The ubiquitin−proteasome system (UPS) plays a critical role in maintaining cellular homeostasis by regulating protein degradation and post-translational modifications in response to various stresses and physiological processes[6]. In recent years, research on the role of the UPS in DNA repair regulation has expanded significantly, drawing increased attention to the potential of modulating DNA repair pathways to improve radiotherapy outcomes[7,8]. Notably, ubiquitination plays a pivotal role in regulating the turnover and activity of targeted proteins, depending on the number and specific sites of ubiquitin attachment. This growing body of research underscores the importance of the UPS in radiotherapy, as it presents new opportunities to enhance therapeutic efficacy by targeting DNA repair mechanisms *via* ubiquitination-related pathways[9]. Based on these findings, our research has focused on exploring the regulatory mechanisms of ubiquitination within the tumor cell nucleus following radiotherapy. Recognizing that K48-linked ubiquitination is generally associated with the degradation of protein substrates, we initially analyzed a range of clinical biomarkers related to nuclear K48-linked ubiquitination in tumor samples collected before and after radiotherapy. Notably, we found that high levels of K48-linked ubiquitin before radiotherapy strongly correlate with favorable therapeutic outcomes. However, radiotherapy appears to induce a progressive decline in this accumulation, suggesting a potential mechanism of resistance to radiotherapy-induced cytotoxicity.

Building on this critical observation, our previous research identified that deubiquitination plays a key role in reducing K48-linked ubiquitin accumulation, which in turn contributes to the diminished effectiveness of radiotherapy[10]. However, this finding primarily addresses the "clearance" aspect of the process. The role of E3 ubiquitin ligase-mediated "production" in this downregulation remains unclear. Therefore, the primary objective of this study is to investigate the regulatory role of nuclear E3 ligases and their influence on this process. To further explore the role of E3 ligases in the aforementioned regulatory processes, we employed a class of broad-spectrum E3 ligase-binding small molecules tocapture nuclear E3 ligases from tumor cells both before and after radiotherapy, enabling the identification of differential and potentially key regulators involved in this process. Our findings revealed that Nitrogen Permease Regulator-Like 2 (NPRL2), a component of the GAP Activity Towards Rags 1 (GATOR1) complex, associates with specific nuclear E3 ligases after radiotherapy, mediating the downregulation of nuclear K48-linked ubiquitin accumulation. Further investigation revealed that the E3 ligases interacting with NPRL2 are likely involved in HR or NHEJ repair mechanisms following radiotherapy. Notably, Ring Finger Protein 8 (RNF8) and Ring Finger Protein 168 (RNF168) play crucial roles in the initial response to DSBs and are essential for the proper execution of both HR and NHEJ pathways[10,11]; HECT (homologous to the E6AP carboxyl terminus), UBA (ubiquitin-associated) and WWE domain containing 1 (HUWE1)-mediated neddylation of DNA-dependent protein kinase catalytic subunit (DNA-PKcs) supports NHEJ processes[12]. Importantly, NPRL2 sequesters these E3 ligases by binding to their ubiquitination functional domains, thereby inhibiting their ubiquitination activity. This inhibition contributes to sustained HR and NHEJ repair. Collectively, these findings suggest that NPRL2's negative regulation of nuclear E3 ligases enhances DNA repair, ultimately contributing to radioresistance in CRC.

Together with DEP domain containing 5 (DEPDC5) and nitrogen permease regulator-like 3 (NPRL3), NPRL2 is part of GATOR1 complex. GATOR1 exhibits GTPases-activating protein (GAP) activity, which inactivates Rag GTPases and negatively regulates mammalian target of rapamycin C1 (mTORC1) signaling in response to amino acid deprivation[13]. Under normal conditions, the spatiotemporal distribution of NPRL2 is tightly regulated, with the protein typically localized in the cytoplasm, where the GATOR1 complex is primarily active. However, our

findings reveal that following radiotherapy, NPRL2 translocates to the nucleus and plays a critical role in promoting radiotherapy resistance in patients with LARC, consistent with the novel mechanism we have identified. These observations underscore the need for further investigation into how alterations in NPRL2's spatiotemporal dynamics contribute to this resistance.

Adenosine monophosphate-activated protein kinase (AMPK) is a pivotal cellular energy sensor and regulator, activated by elevated AMP/ATP and ADP/ATP ratios under conditions of metabolic stress. AMPK inhibits mTORC1 by phosphorylating and activating tuberous sclerosis complex 2 (TSC2) and by phosphorylating Raptor, a key component of mTORC1[14]. Moreover, AMPK-mediated phosphorylation of WD repeat domain 24 (WDR24), a component of the GAP activity towards Rags 2 (GATOR2) complex, modulates glucose-induced mTORC1 activation[15]. The GATOR2 complex, consisting of Meiosis regulator and mTOR interacting protein (MIOS), SEC13 homolog of *S. cerevisiae* (SEC13), SEH1-like nucleoporin (SEH1L), WDR24, and WD repeat domain 59 (WDR59), directly interacts with and suppresses the GATOR1 complex[15,16].

Additionally, AMPK is involved in processes related to radiotherapy. AMPK was found to be highly activated in radioresistant colorectal cancer patients, and its suppression sensitizes CRC cells to radiotherapy[17]. Ionizing radiation (IR) induced phosphorylation and activation of AMPK in tumor cells. AMPK is involved in the ATM−AMPK−p21 pathway, regulates the IR-induced G2/M checkpoint, and may be targeted by metformin to enhance radiation responses[18]. Recently, several studies have demonstrated that AMPK is involved in DSB repair. AMPK promotes NHEJ in DSB repair by recruiting tumor protein *P*53-binding protein 1 (53BP1), which facilitates the joining of distant DNA ends during the damage response[19].

In this study, we demonstrated that NPRL2 dissociation from the GATOR1 complex and its subsequent nuclear translocation upon radiotherapy are mediated by the AMPK/WDR24 signaling axis. Inhibition of AMPK impairs DNA repair by preventing NPRL2 nuclear translocation, thereby sensitizing CRC cells to radiotherapy. Our findings offer a promising strategy to enhance the radiosensitivity of CRC in clinical applications.

2. Materials and methods

2.1. Cell culture

HCT116, DLD-1 cell lines, purchased from American Type Culture Collection (Manassas, VA, USA), were cultured in RPMI-1640, supplemented with 10% fetal bovine serum and 1% penicillin−streptomycin. Cells were maintained at 37 °C in 5% CO_2. All cell lines were authenticated by short tandem repeat analysis at China Center for Type Culture Collection (Wuhan, China), and the absence of mycoplasma contamination was verified using a PCR detection kit. Cells were frozen in liquid nitrogen and used for experiments at passages 3 to 10 after thaw.

2.2. Lentiviral transduction and transient transfection

The coding sequences of full-length human *WDR24* and *NPRL2* were inserted into the pCDNA3.0 vector with a FLAG tag. Additionally, *DEPDC5* and *NPRL2* were inserted into the pCDNA4.0 vector with a Myc tag, while *SEH1L* and *WDR24* were inserted into pCDNA3.0 with an HA tag.

The CRISPR-KO cell lines were constructed by cloning single-guide RNAs (sgRNAs) targeting *NPRL2* (sg: 5′-GCAGAGGCTGGCCATACCAA-3′), *DEPDC5* (sg: 5′-AAGGATCAGTATATTGGCCG-3′), *WDR59* (sg: 5′-GGGACATTGGAGCTGTGCAG-3′), *SEC13* (sg: 5′-GGTGTCAGTAATTAACACTG-3′), *WDR24* (5′-GCACAGCTCAGGTTAAGCGA-3′), *PRKAA1* (the gene encoding AMPKα1, sg: 5′-GCAACTATCGATCTTGCCAA-3′), *PRKAA2* (the gene encoding AMPKα2, sg: 5′-GAAGAGTTGAGTACGCGCTC-3′) and Negative Control (Scrambled, sg: 5′-CGAGCTTGACTACTTGGCAA-3′) into the lentiCRISPRv2 backbone (Addgene [Watertown, MA, USA] plasmid No. 52961).

Lentiviruses were produced by co-transfecting the above constructs, psPAX2 and pMD2.G plasmids, into HEK293T cells. The viruses were then transduced into CRC cells, followed by puromycin selection to generate stable cell lines.

The full length of *NPRL2* and truncated *HERC2* (2759−3222 aa, 3223−3597 aa, 3598−4004 aa, 4005−4414 aa, 4415−4834 aa [HERT]) were cloned into pcDNA3.1 vector tagged with Myc. Truncated *RNF8* (1−92 aa, 93−180 aa, 181−260 aa, 261−360 aa, 361−441 aa [RING]), truncated *HERC2* (2759−3222 aa, 3223−3597 aa, 3598−4004 aa, 4005−4414 aa, 4415−4834 aa [HERT]), truncated *HUWE1* (3404−3758 aa, 3759−4037 aa, 4038−4374 aa [HECT]).

2.3. X-ray radiation treatment

At room temperature, X-ray exposure at a dose rate of 1.18 Gy/min (160 kV, 25 mA, 0.3 mm Cu filter) was applied to cells in the logarithmic growth phase using an RS 2000 X-ray biological irradiator (Rad Source Technologies, Weihai, China). All cells requiring irradiation were given a single dose of 6 Gy. Cell samples were collected at the corresponding time points after radiotherapy (see Results section).

2.4. Human samples

This study was approved by the Institutional Ethics Committees of the First Affiliated Hospital of Sun Yat-sen University (SYSUFAH) and Sun Yat-sen University Cancer Center (SYSUCC), and conducted in accordance with the Declaration of Helsinki. Written informed consent was obtained from each patient. We collected tumor tissue samples from LARC patients before and after radiotherapy at two centers, SYSUCC and SYSUFAH. Patients were eligible for inclusion if they were 18 years or older, had a pathological diagnosis of LARC, and had previously undergone radiotherapy, regardless of sex. Patients at the SYSUCC center received radiotherapy between 2000 and 2015, whereas the radiotherapy center at SYSUFAH was established later, with treatments occurring from 2017 to 2020. Consequently, the follow-up period at SYSUFAH is relatively shorter. All patients at both centers underwent neoadjuvant chemoradiotherapy, followed by surgical treatment (mainly Miles and Dixon procedures). Some patients received adjuvant chemotherapy after surgery. The radiotherapy regimen was long-course radiotherapy, with a prescribed dose of 50 Gy in 25 fractions.

After CRT, TRG grading was based on the 4-tier classification described in the 8th edition of the AJCC guidelines, defined as follows: TRG 0 indicates no viable cancer cells (complete response); TRG 1 indicates single cells or rare small clusters of cancer cells (near complete response); TRG 2 indicates residual cancer with visible tumor regression, though more than just single

cells or small clusters are present (partial response); and TRG 3 indicates extensive residual cancer with no visible tumor regression (poor or no response)[20].

2.5. Histology and immunohistochemistry (IHC) assays

Tissue specimens were fixed in buffered 10% formalin for 24 h followed by paraffin embedding. Next, 4-mm-thick sections were prepared for histology and IHC assays. Tissue sections were deparaffinized and then rehydrated before undergoing antigen retrieval and inactivation of endogenous peroxidase. The specimens were incubated overnight at 4 °C with primary antibodies diluted 1:100−200 after blocking with blocking buffer (1 × PBS, 10% normal goat serum, and 0.3% Triton X-100) for 1 h. The next day, sections were incubated for 1 h at room temperature with an HRP-conjugated secondary antibody, visualized with an Envision Detection Kit, and counterstained with hematoxylin.

The Immunoreactive Score (IRS) was used for the analysis of IHC marker expression. In brief, the percentage of protein-positive cells was divided into four categories (<10%, 11%−50%, 51%−80%, and >80%, with corresponding scores of 1, 2, 3, and 4, respectively). The staining intensity was given a value between 0 (no detectable immunostaining) and 3 (strong immunostaining). The IRS (0−12) was then calculated by multiplying the score values. If an examined sample stained heterogeneously for IHC markers, then the staining intensity of each component was scored independently, and the results were summed[8].

2.6. Mass spectrometry analysis

HCT116 cells were cultured and divided into two groups: non-ionizing radiation (Non-IR) and IR treatment. Cells in the IR group were exposed to IR and collected 2 h post-treatment.

Cells were washed with ice-cold PBS and lysed using nuclear and cytoplasmic extraction reagents to obtain nuclear proteins according to the manufacturer's instructions. Nuclear proteins were affinity-labeled with E3 ligase ligand-8-biotin. The biotin-labeled nuclear proteins were then enriched through streptavidin affinity purification. The purified protein samples were separated using SDS-PAGE, after which the gel bands corresponding to nuclear proteins were excised for analysis. These excised bands were digested into peptides and analyzed by liquid chromatography-tandem mass spectrometry (LC−MS/MS). Proteins were identified and quantified based on the unique peptides detected and their molecular masses.

2.7. Co-immunoprecipitation (Co-IP) and Western blot (WB) assays

Cells were washed with ice-cold PBS and lysed using nuclear and cytoplasmic extraction reagents (No. 78835, Invitrogen) to obtain nuclear proteins and cytoplasmic proteins, according to the manufacturer's instructions. Protein concentration was quantified using a BCA protein assay kit.

For Co-IP, cell lysates were incubated overnight at 4 °C with either antibody-conjugated beads or with specific primary antibodies. For samples treated with primary antibodies, it was followed by incubation with protein G agarose beads for 2 h at 4 °C. After washing, the pulldown products were subjected to SDS-PAGE. For WB assay, protein separated by SDS-PAGE were transferred to a PVDF membrane, and the membrane was blocked with 5% milk in TBS and incubated overnight at 4 °C with specific primary antibodies. This was followed by incubation with HRP-conjugated secondary antibodies. Signals were visualized using an enhanced chemiluminescence reagent and captured with a ChemiDoc IRS system (Bio-Rad), and quantified using ImageJ software.

2.8. Protein docking between NPRL2 and RNF8, HUWE1, Herc 2 based on structure

The predicted protein structures of NPRL2 (identifier: AF-Q8WTW4-F1, covering residues 1−380), RNF8 (identifier: AF-O76064-F1, covering residues 1−485), and HERC2 (identifier: AF-A0A0G2JPS8-F1, covering residues 4424−4834) were downloaded from Alphafold Protein Structure Database (https://alphafold.ebi.ac.uk/). The structure of HUWE1 was downloaded from the Protein Data Bank (PDB ID: 3H1D, covering residues 3980−4096 and 4102−4366). The protein structure was prepared with MOE2019.0102, and protein−protein docking was performed by Vakser Lab (https://gramm.compbio.ku.edu/). NPRL2 acted as receptor, while RNF8, HUWE1, and HERC2 acted as ligands for free docking. Interaction results were visualized using MOE2019.0102.

2.9. HR and NHEJ reporter assays

The reporter constructs for HR and NHEJ, as well as the I-SceI expression plasmid pCMV-NLS-I-SceI, were gifts from Dr. Lin Feng at the Sun Yat-sen University Cancer Center (SYSUCC, Guangzhou, China). Briefly, parent cells were transfected with the DR-GFP (HR) or EJ5-GFP (NHEJ) reporter plasmid and pCMV-NLS-I-SceI plasmid; NPRL2-WT or NL2-PRKO cells were transfected with the DR-GFP (HR) or EJ5-GFP (NHEJ) reporter plasmid, pCMV-NLS-I-SceI plasmid, pCMV-DsRed plasmids (as an internal reference to monitor transfection efficiency). Meanwhile, the transfection system in the absence of pCMV-NLS-I-SceI plasmid was set as a negative control. Transfection was accomplished *via* electroporation with a DT-130 program using the kit (V4XP-2032) on a Lonza 4D machine (Lonza, Cologne, Germany). 36 h after transfection, cells were harvested and re-plated. After 12 h, cells were treated with drugs at the indicated concentration for an additional 12 h and then collected for analysis of DNA repair efficiency (presented as the GFP^+ rate for parent cells or the relative ratio of GFP^+/$DsRed^+$ cells for NPRL2-WT or NPRL2-KO HCT116 cells) on a CytoFLEX flow cytometer.

2.10. Immunofluorescence (IF) assay

CRC cells on confocal dishes were fixed with 4% paraformaldehyde for 20 min at room temperature, then permeabilized using 0.5% Triton X-100 in PBS and blocked with 3% goat serum for 1 h at 37 °C. The cells were then incubated with primary antibodies at 4 °C overnight, followed by incubation with fluorescent secondary antibodies at room temperature for 1 h. Cell nuclei were stained with DAPI for 2 min. Images were acquired using an LSM880 with Airyscan FAST Confocal microscopy (ZEISS, Oberkochen, Germany). The quantitative analysis was carried out by counting the number of foci per cell/cell nucleus.

2.11. *Colony formation assay*

The colony formation assay was performed as described previously[8,10,21]. Briefly, CRC cells were seeded into 6-well plates at a density of 1000 cells/well. After 24 h, the cells were treated with X-rays or inhibitors and cultured for 10−14 days. They were fixed in methanol, and subsequently stained with 0.5% crystal violet. Colonies containing more than 50 cells were counted. Plating efficiency (PE) and the survival fraction (SF) were calculated using Eqs. (1) and (2):

$$\mathrm{PE}\ (\%) = \text{Number of colonies formed}/\text{Number of cells seeded} \times 100 \quad (1)$$

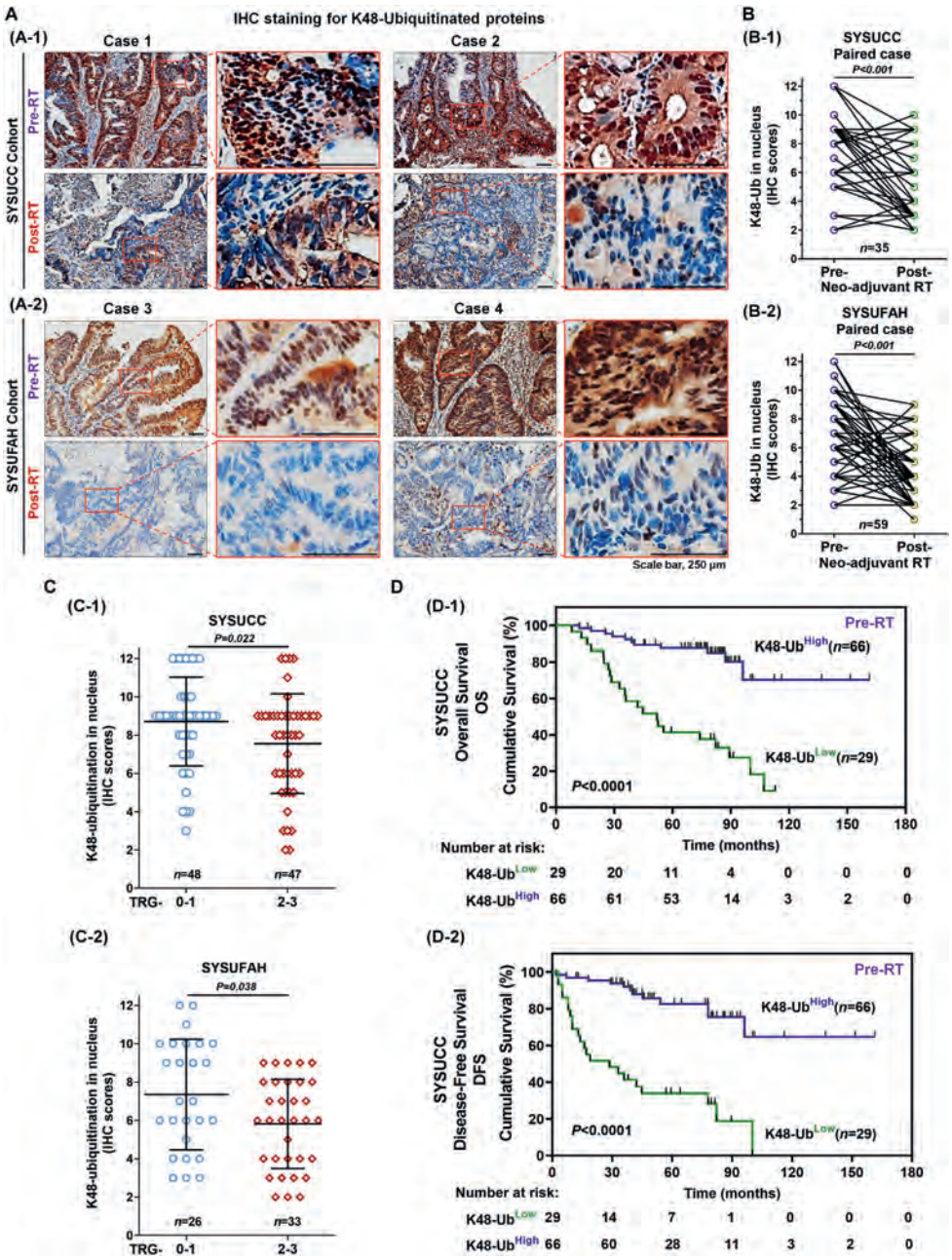

Figure 1 Radiotherapy-induced downregulation of nuclear K48-Ub in response to radiation stress and survival adaptation in CRC. (A) IHC analysis of K48-ubiquitinated proteins in pre- and post-CRT CRC tissue samples from (A-1) SYSUCC cohort and (A-2) SYSUFAH cohort. Representative images of cases are shown. (B) The IHC scores for nuclear K48-ubiquitination in paired cases of CRC before and after CRT in (B-1) SYSUCC cohort (n = 35) and (B-2) SYSUFAH cohort (n = 59). A line connects each pair of pre- and post-treatment samples. Statistical significance was determined using the Wilcoxon signed-rank test (non-normal distribution). (C) The IHC scores for K48-ubiquitination in the nucleus of two groups of TRG grades in CRC samples from (C-1) SYSUCC cohort (n = 95) and (C-2) SYSUFAH cohort (n = 59). Data are represented as mean ± SD. Statistical significance was determined by Mann−Whitney U test (non-normal distribution). (D) Kaplan−Meier survival curve depicts the (D-1) overall survival and (D-2) disease-free survival of patients with CRC from SYSUCC cohort (n = 95) before CRT. The cohorts are divided into high and low groups according to K48-Ub IHC scores. Statistical significance was determined by log-rank test.

$$SF = \text{Number of colonies formed after irradiation} / \times (\text{Number of cells seeded} \times PE) \quad (2)$$

2.12. Nude mouse xenograft model and experimental therapy

All animal experiments were approved by the Animal Welfare and Ethics Committee of Jinan University (Approval No. 20240227-0076) and conducted in the Central Laboratory of the Overseas Chinese Hospital affiliated to Jinan University.

Female BALB/c nude mice (4−5 weeks old, 15−18 g; SLRC Laboratory Animal Co., Shanghai, China) were subcutaneously inoculated in the right flank with 1×10^6 NPRL2-WT or NPRL2-KO HCT116 cells to establish xenografts; or 1×10^6 NPRL2-WT or NPRL2-OE HCT116 cells to establish xenografts. When tumor volumes reached ∼100 mm^3 (calculated as $0.52 \times width^2 \times length$) of NPRL2-WT or NPRL2-KO groups, mice received alternating treatments of the test drug and X-ray irradiation. When tumor volumes reached ∼250 mm^3 (calculated as $0.52 \times width^2 \times length$) of NPRL2-WT or NPRL2-OE groups, mice received alternating treatments of the test drug and X-ray irradiation. Mice were euthanized 1−2 weeks post-treatment, and tumors were excised, weighed, and processed for pathological analysis.

2.13. Statistical analysis

All *in vitro* experiments were conducted at least three times. Data are presented as the mean ± standard deviation (SD). Statistical analyses were performed using GraphPad Prism 7.0 or SPSS 20.0. For data with a normal distribution, comparisons between two groups were evaluated using a two-tailed Student's *t*-test (two-sample *t*-test), while comparisons among multiple groups were assessed using two-way ANOVA (two-factor analysis of variance). Given the non-normal distribution of IHC scores, paired samples before and after radiotherapy were analyzed using the Wilcoxon

Table 1 Correlation between levels of K48-Ub and clinicopathological parameters for pre-RT samples.

Variables	No. of patients (%)	K48-Ub levels		Hazard ratio (95% CI)	*P* value
		Low (*n*; %)	High (*n*; %)		
Gender					0.483
Male	51 (53.7)	14 (14.7)	37 (38.9)	0.861 (0.558−1.328)	
Female	44 (46.3)	15 (15.8)	29 (30.5)	1.177 (0.754−1.837)	
Age					0.713
≤55	42 (44.2)	12 (12.6)	30 (31.6)	0.910 (0.548−1.512)	
>55	53 (55.8)	17 (17.9)	36 (37.9)	1.075 (0.737−1.567)	
Pthologic grade					0.203
I	12 (12.6)	1 (1.1)	11 (11.6)	−	
II	65 (68.4)	22 (23.2)	43 (45.3)	−	
III	18 (19.0)	6 (6.3)	12 (12.6)	−	
cT grade					0.659
T2	5 (5.3)	2 (2.1)	3 (3.2)	−	
T3	49 (51.6)	13 (13.7)	36 (37.9)	−	
T4	41 (43.1)	14 (14.7)	27 (28.4)	−	
cN					0.897
N0	31 (32.6)	10 (10.5)	21 (22.1)	−	
N1	52 (54.7)	16 (16.8)	36 (37.9)	−	
N2	12 (12.7)	3 (3.2)	9 (9.5)	−	
CEA (ng/mL)					0.643
<5	59 (62.1)	17 (17.9)	42 (44.2)	0.921 (0.645−1.315)	
≥5	36 (37.9)	12 (12.6)	24 (25.3)	1.138 (0.664−1.949)	
CA19-9(Ku/L)					0.954
≤35	75 (78.9)	23 (24.2)	52 (54.7)	1.007 (0.805−1.260)	
>35	20 (21.1)	6 (6.3)	14 (14.7)	0.975 (0.417−2.284)	
Adjuvant chemotherapy					
No	34 (35.8)	11 (11.6)	23 (24.2)	1.088 (0.615−1.926)	0.773
Yes	61 (64.2)	18 (18.9)	43 (70.5)	0.953 (0.682−1.332)	
Surgical procedure					0.68
Dixon	64 (67.4)	18 (18.9)	46 (48.4)	−	
Miles	27 (28.4)	10 (10.5)	17 (17.9)	−	
Hartmann	4 (4.2)	1 (1.1)	3 (3.2)	−	
TRG					**0.049**
0	26 (27.4)	4 (4.2)	22 (23.2)	−	
1	22 (23.2)	7 (7.4)	15 (15.8)	−	
2	31 (32.6)	9 (9.5)	22 (23.2)	−	
3	16 (16.8)	9 (9.5)	7 (7.4)	−	
Status					**< 0.001**
Alive	62 (65.3)	7 (7.4)	55 (57.9)	0.290 (0.151−0.557)	
Dead	33 (34.7)	22 (11.6)	11 (11.6)	4.552 (2.556−8.107)	

cT: clinical T stage; cN: clinical N stage. *P*-value in bold indicates a statistically significant difference ($P < 0.05$).

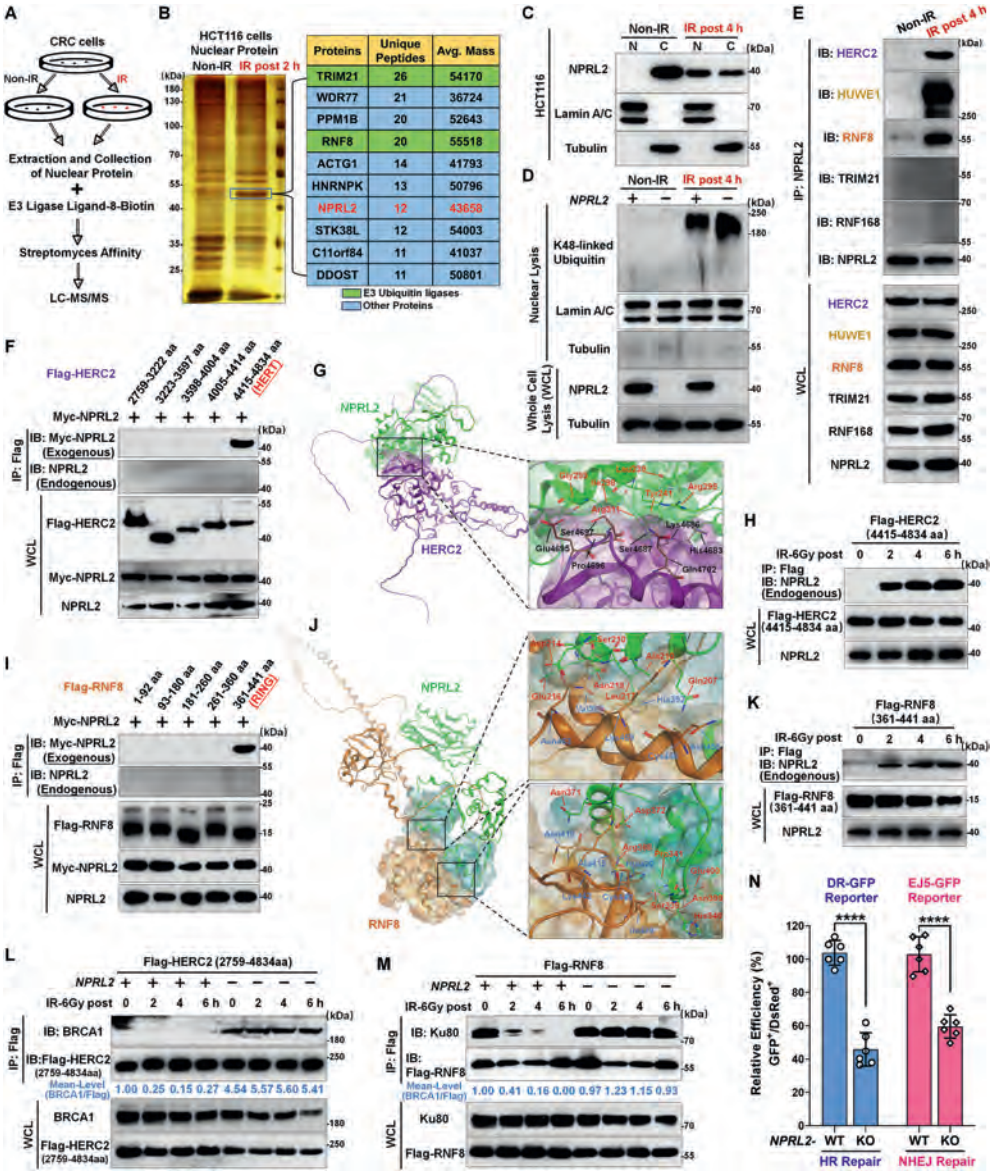

Figure 2 NPRL2 is identified as a factor that translocates into the nucleus upon RT treatment, where it hijacks degradative E3 ubiquitin ligases to enhance DNA repair. (A) Schematic illustration for the identification of proteins interacting with E3 ligase with LC−MS/MS in CRC cells. (B) LC−MS/MS analysis was conducted to identify proteins interacting with E3 ligase in HCT116 cells 2 h after 6 Gy IR. Nuclear proteins were extracted from non-irradiated (Non-IR) and irradiated (IR) HCT116 cells. Proteins were identified as differentially expressed or modified in response to irradiation. The table on the right lists the identified proteins, including E3 ubiquitin ligases (highlighted in green) and other proteins (highlighted in blue), along with the number of unique peptides detected and their average molecular masses. Notably, the NPRL2 protein (highlighted in red) showed a distinct interaction pattern. (C) WB analysis was performed to detect subcellular localization of NPRL2 in HCT116 cells following 6 Gy IR, with cells collected 4 h post-irradiation. Nuclear (N) and cytoplasmic (C) fractions were extracted from cells. (D) WB analysis of K48-ubiquitination and NPRL2 expression in nuclear and whole-cell lysates under Non-IR and IR conditions. Cells were treated with 6 Gy IR, and cells were collected at the 4 h time point. (E) Co-IP and WB analysis of interaction of Flag-NPRL2 with E3 ligase in the nucleus (HERC2, HUWE1, and RNF8) under Non-IR and IR conditions. Cells were treated with 6 Gy IR, and cells were collected at the 4 h time point. (F) Co-IP of Flag-tagged HERC2 protein fragments with Myc-NPRL2. HCT116 cells were transfected with various truncated Flag-HERC2 (2759−3222 aa, 3223−3597 aa, 3598−4004 aa, 4005−4414 aa, 4415−4834 aa) and co-transfected with Myc-NPRL2. (G) Molecular docking model of the interaction between NPRL2 and HERC2. The zoomed-in view on the right highlights the key interacting residues at the interface of NPRL2 and HERC2. (H) Co-IP of Flag-HERC2 (4415−4834 aa) protein fragments with NPRL2 after IR. Cells were collected at specific time points (0, 2, 4, 6 h) after 6 Gy IR. HCT116 cells were transfected with truncated Flag-HERC2 (4415−4834 aa). (I) Co-IP of Flag-tagged RNF8 protein fragments with Myc-NPRL2. HCT116 cells were transfected with various truncated Flag-RNF8 (1−92 aa, 93−180 aa, 181−260 aa, 261−360 aa, 361−441 aa) and co-transfected with Myc-NPRL2. (J) Molecular docking model of the interaction between NPRL2 and RNF8. The zoomed-in view on the right highlights the key interacting residues at the interface of NPRL2 and RNF8. (K) Co-immunoprecipitation (Co-IP) of Flag-RNF8 (361−441 aa) protein fragments with NPRL2 after IR. Cells were collected at specific time points (0, 2, 4, 6 h) after 6 Gy IR. HCT116 cells were transfected with truncated Flag-RNF8 (361−441 aa). (L) Co-IP of Flag-HERC2 (2759−4834 aa) protein fragments with NPRL2 after

signed-rank test. At the same time, comparisons between two independent groups were performed using the Mann−Whitney U test. Relationships between clinical categorical variables were analyzed using the chi-square test. Survival times for patient groups were assessed using the log-rank test, Kaplan−Meier curves, and the Cox proportional hazards model. The relationship between K48-linked ubiquitin and NPRL2 expression was evaluated using Spearman correlation analysis. A *P*-value of less than 0.05 was considered statistically significant.

All information regarding reagents, plasmids, antibodies, cell constructs, and software can be found in Supporting Information Table S1.

3. Results

3.1. Radiotherapy-induced downregulation of nuclear K48-Ub in response to radiation stress and survival adaptation in CRC

The level of intracellular ubiquitination generally maintains a dynamic equilibrium, but external factors can disrupt this balance, prompting a cellular stress response. Ubiquitination modifications, such as K48 and K11 linkages, are typically associated with protein degradation and mediate the targeted degradation of specific proteins[22,23]. Consequently, under stress conditions, cellular outcomes are often influenced by the regulation of these degradative ubiquitination processes. Therefore, the equilibrium levels of ubiquitination modifications before stress may predict different outcomes[24]. Since the primary biological effect of radiotherapy is DNA damage, the cellular response to this damage, which is tightly regulated by ubiquitination-related pathways, is a key determinant of radiosensitivity. Therefore, we focus on characterizing nuclear degradative ubiquitination levels to gain deeper insight into its role in the cellular response to radiotherapy.

To assess the comprehensive impact of radiotherapy on nuclear K48-linked protein ubiquitination (K48-Ub) levels, we first characterized tumor tissues from patients with LARC. The immunohistochemistry (IHC) scores of K48-Ub were obtained from paired pre- and post-treatment CRC samples in two independent cohorts, the SYSUCC and SYSUFAH cohorts. In both cohorts, we found that nuclear K48-Ub levels were significantly decreased in CRC cells after radiotherapy (RT) (Fig. 1A and B). This suggests that radiotherapy can downregulate nuclear K48-Ub levels. Additionally, the heatmap analysis showed that patients with high nuclear K48-Ub expression tend to have lower tumor regression grades (TRG) before RT (Supporting Information Fig. S1A and S1B). TRG is used to assess the response of tumors to neoadjuvant therapy, with higher grades indicating less tumor regression[20]. In SYSUCC cohort, higher nuclear K48-Ub levels before RT were significantly associated with lower TRG (Table 1). Patients with TRG 0-1 showed significantly higher nuclear K48-Ub levels than those with TRG 2-3 (Fig. 1C). The findings mentioned above suggest a positive correlation between nuclear K48-Ub levels prior to radiotherapy and sensitivity to radiotherapy.

In addition to assessing the correlation between nuclear K48-Ub levels and clinicopathological parameters, we further analyzed the prognostic influence of nuclear K48-Ub. The results showed that higher nuclear K48-Ub levels before RT were significantly associated with a favorable prognosis and lower TRG (Table 1). Specifically, higher nuclear K48-Ub levels were significantly correlated with longer overall survival (OS) and disease-free survival (DFS) before RT in the SYSUCC cohort (Fig. 1D). Moreover, both univariate and multivariate regression analyses indicated that pre-RT nuclear K48-Ub levels can independently serve as a prognostic factor for patient survival (Supporting Information Table S2). Notably, in this cohort, after RT, there was no significant association between nuclear K48-Ub levels and either TRG or prognosis (Supporting Information Tables S3 and S4, Fig. S2A and S2B). However, our findings from the SYSUFAH cohort showed no significant association between nuclear K48-Ub levels and OS or DFS, either before or after RT (Supporting Information Fig. S3). This observation may be attributed to the relatively short follow-up period for these patients, which temporarily hinders the emergence of a definitive pattern.

In summary, stable levels of nuclear K48-Ub prior to the initiation of radiotherapy suggest a potential correlation with prognosis. Taken together, these results suggest that the radiotherapy-induced reduction in nuclear K48-Ub levels is a critical event in the radiation response, contributing to poorer survival outcomes.

3.2. NPRL2 is identified as a factor that translocates into the nucleus upon RT treatment, where it hijacks degradative E3 ubiquitin ligases to enhance DNA repair

As previously noted, RT induces a reduction in nuclear K48-Ub levels, necessitating a thorough investigation into the underlying drivers and mechanisms responsible for this decrease. Our previous studies have demonstrated that RT enhances the activity of nuclear deubiquitinases, which likely play a significant role in the reduced accumulation of nuclear ubiquitinated proteins[10]. This process involves the removal of ubiquitin chains from their target proteins. However, whether RT directly impacts the ubiquitination process itself remains uncertain. Given that the nucleus contains numerous E3 ubiquitin ligases, a focused investigation into whether RT influences the regulatory mechanisms governing their activity is warranted. Ubiquitin E3 ligases are critical components of the ubiquitination process, playing a key role in targeting proteins due to their stringent control over both the efficiency and substrate specificity of the ubiquitination reaction[25]. To investigate the effects of RT on nuclear ubiquitination processes, we used E3 Ligase Ligand-8, a biotinylated small molecule with broad binding affinity for E3 ubiquitin ligases. Through streptavidin affinity capture, we isolated nuclear

IR. Cells were collected at specific time points (0, 2, 4, 6 h) after 6 Gy IR. HCT116 cells were transfected with truncated Flag-HERC2 (2759−4834 aa) with NPRL2 or not. (M) Co-IP of Flag-RNF8 with NPRL2 after IR. Cells were collected at specific time points (0, 2, 4, 6 h) after 6 Gy IR. HCT116 cells were transfected with Flag-RNF8 and NPRL2 or not. (B−F) and (H, I, K−M), all WB or Co-IP analyses were replicated in triplicate. (N) The HR and NHEJ reporter assays for the analysis of DNA DSB repair pathways in NPRL2-WT or -KO HCT116 cells. Successful repair restores GFP expression, which was quantified by flow cytometry. Statistical data are presented as mean ± SD (Student's *t*-test), $^{****}P < 0.0001$.

E3 ligases along with their associated regulatory complexes (Fig. 2A). The silver-stained SDS-PAGE gel revealed a prominent band at approximately 40−55 kDa, observed specifically in the IR 2 h post-treatment group, which was excised for further LC−MS/MS analysis, identifying nuclear-localized E3 ligases such as RNF8 and TRIM21. The table lists the identified proteins, including the number of unique peptides detected and their average molecular mass (Fig. 2B). Interestingly, NPRL2, traditionally known as a cytoplasmic protein, exhibited significant nuclear enrichment following IR. This observation was further

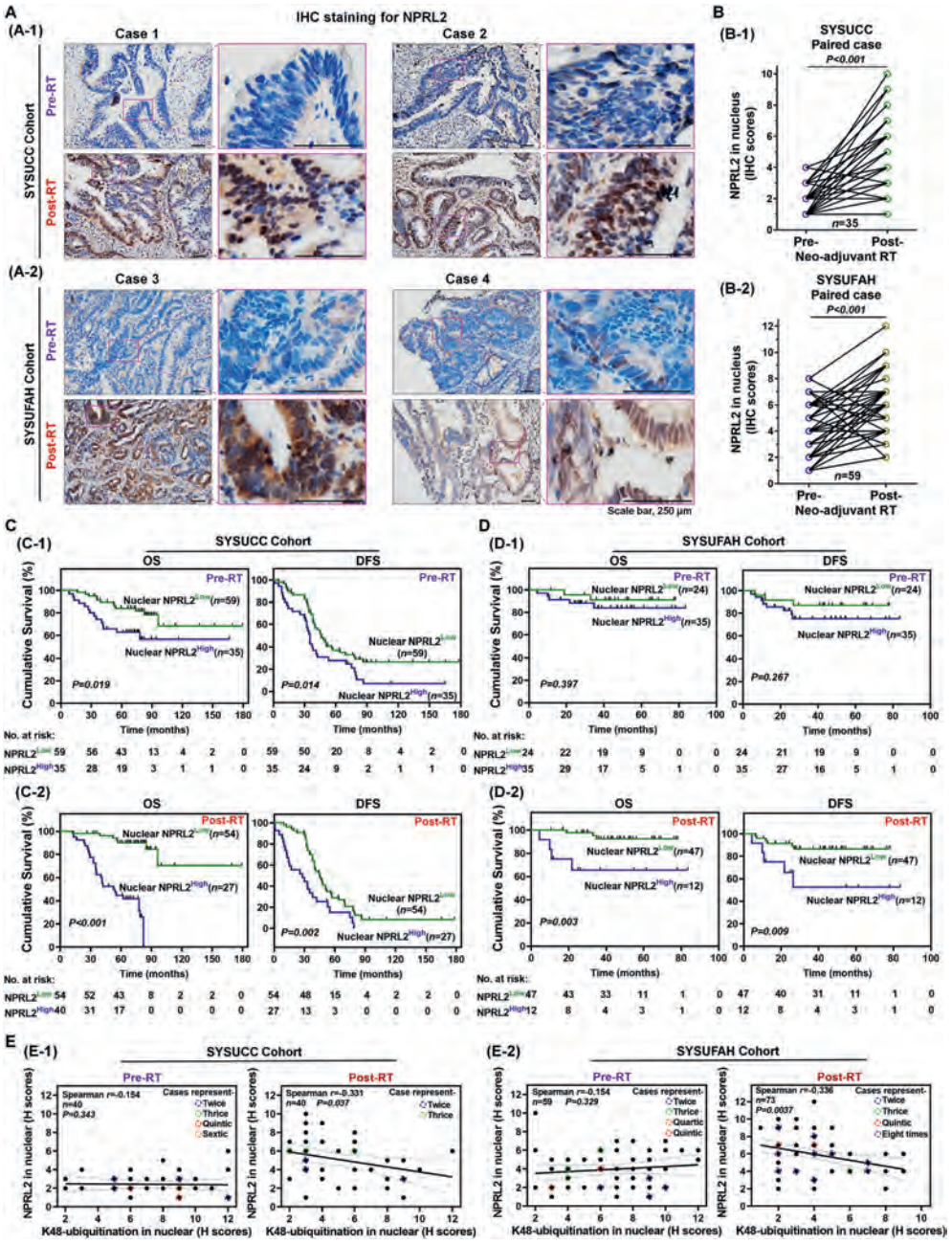

Figure 3 Nuclear translocation of NPRL2 indicates its role in modulating degradative ubiquitination, which impacts the efficacy of LARC radiotherapy. (A) IHC of NPRL2 proteins in pre- and post-CRT CRC tissue samples from the (A-1) SYSUCC cohort and (A-2) SYSUFAH cohort. Representative images of cases are shown. (B) IHC scores for nuclear NPRL2 in paired cases of CRC before and after CRT in (B-1) SYSUCC cohort (n = 35) and (B-2) SYSUFAH cohort (n = 59). A line connects each pair of pre- and post-treatment samples. Statistical significance was determined using the Wilcoxon signed-rank test (non-normal distribution). (C) Kaplan−Meier survival curve depicts the (Left) overall survival and (Right) disease-free survival of patients with CRC from SYSUCC cohort (C-1) pre-CRT (n = 94) and (C-2) post-CRT (n = 81). The cohorts are divided into high and low groups according to NPRL2 IHC scores. Statistical significance was determined by log-rank test. (D) Kaplan−Meier survival curve depicts the (Left) overall survival and (Right) disease-free survival of patients with CRC from SYSUFAH cohort (D-1) pre-CRT (n = 59) and (D-2) post-CRT (n = 59). The cohorts are divided into high and low groups according to NPRL2 IHC scores. Statistical significance was determined by log-rank test. (E) Spearman's correlation between nuclear K48-ubiquitination and NPRL2 levels in the (E−1) SYSUCC cohort and (E−2) SYSUFAH cohort pre- and post-CRT. The number of samples for this figure is annotated on each image.

corroborated by nuclear-cytoplasmic fractionation experiments (Fig. 2C). Moreover, we found that radiation-resistant HCT116 cells inherently exhibit basal nuclear accumulation of NPRL2 even in the absence of irradiation, which is further enhanced following IR exposure (Supporting Information Fig. S4). Together, these results suggest the possibility of novel mechanisms driving NPRL2 nuclear translocation in response to IR. Further validation confirmed that the absence of NPRL2 increases the overall accumulation of nuclear K48-linked ubiquitination after IR (Fig. 2D), indicating that NPRL2 may regulate the function and activity of E3 ligases upon entering the nucleus. Following radiotherapy, NPRL2 interacts with the HECT and RLD domains, which are found in E3 ubiquitin ligases: HERC2, HUWE1, and RNF8 (Fig. 2E). Specifically, NPRL2 interacts with the domain comprising residues 4683−4702 of HERC2; two discrete domains of RNF8 spanning residues 389−392 and 455−463, as well as residues 418−442; and residues 4071−4077 of HUWE1 (Fig. 2G and J, Supporting Information Fig. S5A and S5B). Nevertheless, an intriguing phenomenon was observed: C-terminal truncation mutants of E3 ligases such as HERC2, RNF8, and HUWE1 exhibited binding only to exogenously introduced (overexpressed) NPRL2, but not to endogenous NPRL2 (Fig. 2F and I, Fig. S5A). Remarkably, we observed timely binding of these truncation mutants with endogenous NPRL2 after RT (Fig. 2H and K, Fig. S5C). This observation aligns with the finding that RT induces the interaction between NPRL2 and these E3 ligases, suggesting that temporal and spatial constraints may affect NPRL2 after RT. This phenomenon indicates that the barrier preventing NPRL2 from entering the nucleus to interact with E3 ligases is alleviated after RT induction.

The impact of NPRL2's interaction with the ubiquitination domains of degradative E3 ligases on their downstream substrates—particularly within the DNA repair pathway—remains to be elucidated. To further explore this mechanism, we conducted interaction analyses. Our findings revealed that after NPRL2 knockout, the interaction between HERC2 and BRCA1 significantly intensified, and this enhanced interaction persisted throughout the RT process without significant alteration. In contrast, in the presence of NPRL2, the binding between HERC2 and BRCA1 gradually weakened as RT progressed, highlighting a stark contrast (Fig. 2L). Furthermore, we observed that the interaction between RNF8 and Ku80 was relatively stable under normal conditions. However, when NPRL2 was present, their interaction was transiently disrupted by RT. In contrast, in the absence of NPRL2, this binding remained stable and unaffected after RT (Fig. 2M). Considering the critical roles of BRCA1 and Ku80 in HR and NHEJ, respectively, we speculate that the knockout of NPRL2 might affect both repair processes. Experimental validation confirmed that NPRL2 knockout significantly reduced HR repair efficiency by more than 50% and decreased NHEJ repair efficiency by approximately 40% (Fig. 2N). These findings underscore the crucial role of NPRL2 in facilitating DNA repair following RT.

3.3. Nuclear translocation of NPRL2 indicates its role in modulating degradative ubiquitination, which impacts the efficacy of LARC radiotherapy

The nuclear translocation of NPRL2 induced by RT is believed to be linked to the degradative E3 ligases, thereby enhancing DNA repair mechanisms to alleviate radiation-induced stress. To evaluate whether the nuclear translocation of NPRL2 influences RT efficacy, further analysis of clinical specimens is essential. In initial comparisons of tumor tissue from two patient cohorts, before and after RT, we observed a significant increase in NPRL2 nuclear localization following RT (Fig. 3A and B). This finding supports the occurrence of RT-induced NPRL2 nuclear translocation in clinical settings. In contrast, our observations suggest that chemotherapy drugs commonly used in neoadjuvant therapy for these patients do not directly induce NPRL2 nuclear translocation in CRC cells (Supporting Information Fig. S6). This finding reinforces the uniquely inducible nature of NPRL2's nuclear translocation by RT, effectively ruling out any influence of chemotherapy on this biological behavior. Next, we investigated the clinical significance of NPRL2 nuclear translocation by analyzing its levels before and after RT and their association with various clinical indicators in patients. Our findings reveal that nuclear NPRL2 levels are significantly correlated with poor patient prognosis, particularly after RT (Supporting Information Tables S5 and S6). Further analysis of survival times revealed that patients in both cohorts consistently had shorter OS and DFS when nuclear NPRL2 levels were elevated. This association became especially pronounced after RT (Fig. 3C and D). In the SYSUCC cohort, higher pre-RT nuclear NPRL2 levels predicted shorter OS and DFS, with this predictive value significantly increasing after RT (Fig. 3C). These findings highlight the critical role of post-RT nuclear NPRL2 levels as key determinants of patient survival outcomes and duration. Furthermore, advanced univariate and multivariate regression analyses reveal that post-RT nuclear NPRL2 levels, along with pathological grade, can each serve as independent prognostic indicators of patient survival (Supporting Information Table S7). In contrast, pre-RT levels was an independent prognostic factor for DFS but not for OS (Supporting Information Table S8). Based on our clinical analyses, we hypothesized that NPRL2 nuclear accumulation plays a crucial role in conferring resistance to radiotherapy. To test this, we artificially overexpressed NPRL2 and observed a substantial increase in its nuclear localization (Supporting Information Fig. S7A), so pronounced that radiation-induced nuclear translocation of NPRL2 was largely masked. This suggested that NPRL2, when present in excess, bypasses regulatory mechanisms and accumulates in the nucleus independently of external stimuli. To determine whether this intrinsic nuclear accumulation directly contributes to radiotherapy resistance, we conducted *in vivo* experiments. Strikingly, NPRL2-overexpressing tumors exhibited significantly enhanced resistance to radiation compared to controls (Fig. S7B), supporting our hypothesis that NPRL2 nuclear enrichment is a key driver of therapeutic insensitivity.

As previously discussed, NPRL2 has been found to be closely associated with the process of nuclear K48-linked ubiquitination. Therefore, it is essential to determine whether the analytical findings from clinical specimens align with those from CRC cell experiments. Upon thorough investigation, we found that nuclear NPRL2 accumulation and K48-linked ubiquitination exhibited a strong negative correlation exclusively following RT; no significant relationship was observed between the two prior to treatment (Fig. 3E). These findings suggest that RT induces NPRL2 translocation into the nucleus, alleviating the accumulation pressure from degradative ubiquitination. This process enhances cellular resistance mechanisms, such as DNA repair, thereby increasing resistance to RT and diminishing its therapeutic efficacy.

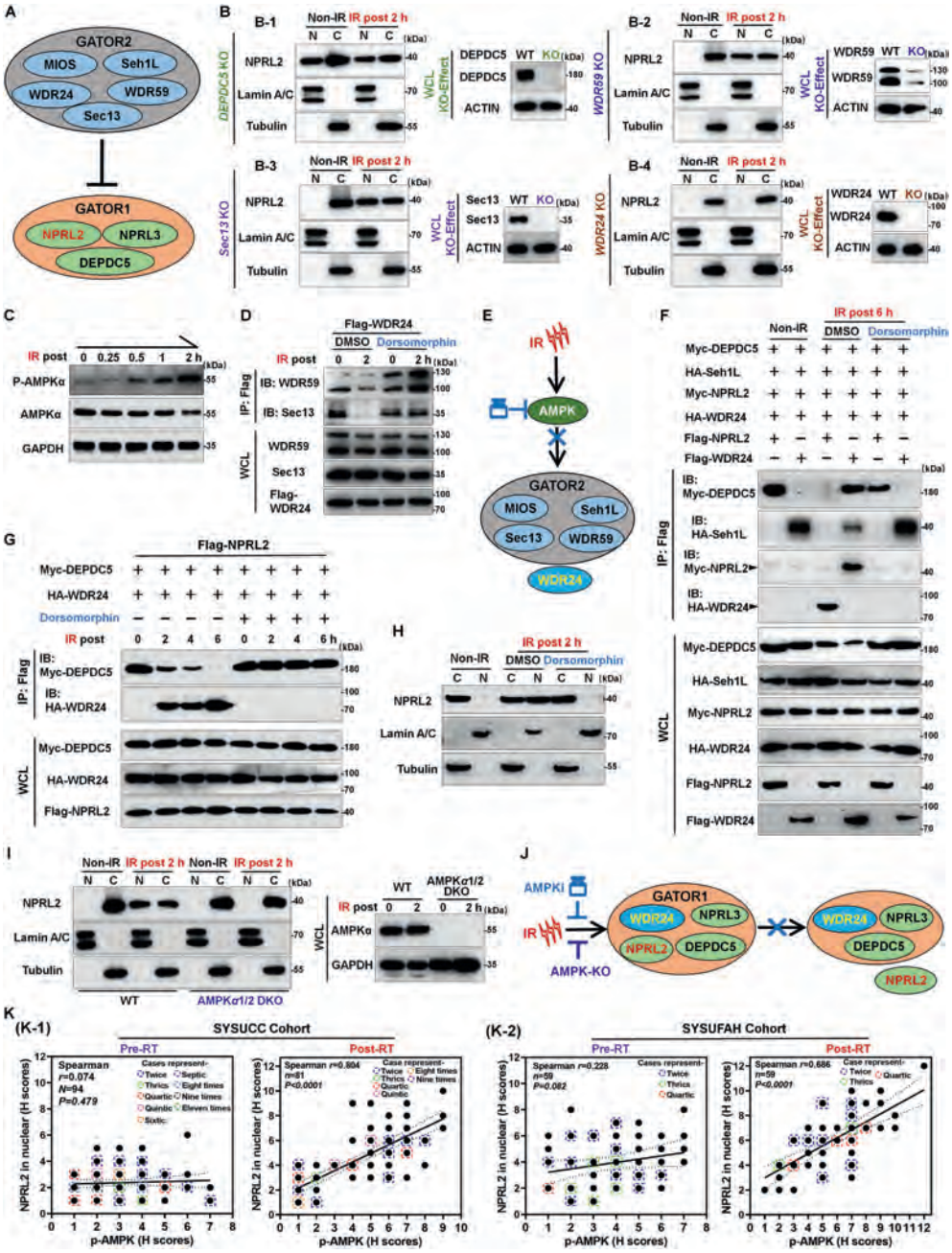

Figure 4 The nuclear translocation of NPRL2 induced by radiation depends on the AMPK/WDR24 axis. (A) Schematic illustration for the GATOR1 and GATOR2 protein complexes. GATOR2 negatively regulates GATOR1. (B) WB analysis of subcellular localization of NPRL2 in (B-1) DEPDC5 KO, (B-2) WDR59 KO, (B-3) Sec13 KO, and (B-4) WDR24 KO HCT116 cells treated with 6 Gy IR, with cells collected 2 h post-irradiation. Nuclear (N) and cytoplasmic (C) fractions were separated and analyzed. WCL WB analysis for knockout effect (Right). (C) WB analysis detecting the level of p-AMPK in HCT116 cells at the indicated time points after 6 Gy IR. (D) Co-IP and WB analysis of the interaction between Flag-WDR24 and WDR59, Sec13 in HCT116 cells 2 h after 6 Gy IR and Dorsomorphin treatment. HCT116 cells were transfected with Flag-WDR24 and treated with Dorsomorphin (10 μmol/L) or DMSO (as a control) for 3 h. (E) Schematic illustration of the AMPK−GATOR2 signaling pathway in CRC cells treated with Dorsomorphin (10 μmol/L) following 6 Gy IR: After radiotherapy, AMPK activation promotes the dissociation of WDR24 from the GATOR2 complex, while the AMPK inhibitor suppresses this process. (F) Co-IP and WB assays detecting the interaction between Flag-NPRL2 or WDR24 and Myc-DEPDC5, HA- SEH1L, Myc-NPRL2, HA-WDR24. These plasmids were transfected into HCT116 cells followed by treatment with Dorsomorphin (10 μmol/L) for 3 h before IR. Cell samples were collected at 6 h time points after 6 Gy IR. (G) Co-IP and WB assays detecting the interaction between Myc-DEPDC5, HA-WDR24, and Flag-NPRL2. These plasmids were transferred into cells followed by treatment with Dorsomorphin (10 μmol/L) for 3 h before 6 Gy IR. Cell samples were collected at the corresponding time points (0, 2, 4, 6 h) after 6 Gy IR. (H) WB analysis detecting the level of NPRL2 in nuclear (N) and cytoplasmic (C) from cells treated with Dorsomorphin (10 μmol/L) for 3 h before IR treatment. Cell samples were collected at 2 h time points after 6 Gy IR. (I) WB analysis detecting the level of NPRL2 in nuclear (N) and cytoplasmic (C) from AMPKα1/2-WT or Double KO HCT116 cells, treated with 6 Gy IR, with cells collected

3.4. The nuclear translocation of NPRL2 induced by radiation depends on the AMPK/WDR24 axis

Having established the biological and clinical significance of RT-induced nuclear translocation of NPRL2, our next objective is to elucidate potential targeted intervention strategies. This involves deciphering the mechanisms by which RT triggers NPRL2 nuclear translocation, aiming to achieve radiosensitization. NPRL2, a pivotal constituent of the GATOR1 complex, plays a central role in modulating its functions. In the context of the mTORC1 pathway, the interplay between GATOR1 and GATOR2 complexes represents a critical regulatory mechanism (Fig. 4A). The competitive and inhibitory interactions among these complexes are primarily driven by the interplay between their key components. Therefore, a comprehensive investigation into the mechanism of NPRL2 dissociation from GATOR1 requires an in-depth exploration of the functions and interactions of the key components within the GATOR1 and GATOR2 complexes. Based on this, we systematically disrupted specific components of the GATOR1 and GATOR2 complexes in CRC cells to investigate their influence on NPRL2's nuclear translocation in response to RT. First, we found that knocking out DEPDC5, a core component of the GATOR1 complex, led to NPRL2 being generally evenly distributed between the nucleus and cytoplasm, regardless of RT (Figs. 4B−1). This observation strongly suggests that the presence of an intact GATOR1 complex is essential for maintaining the spatial regulation of NPRL2. Conversely, when key members of the GATOR2 complex—WDR59 and SEC13—were individually knocked out, we did not observe any significant alteration in RT-induced nuclear translocation of NPRL2 (Figs. 4B−2/3). Interestingly, knockout of WDR24, a crucial GATOR2 component, prevented NPRL2 from translocating to the nucleus in response to RT, resulting in its exclusive retention in the cytoplasm (Fig. 4B-4). This finding suggests that WDR24 plays a critical role in mediating the interaction between NPRL2 and the GATOR1 complex, thereby influencing NPRL2's cellular distribution under RT conditions. Based on these findings, we propose that WDR24 within the GATOR2 complex is intricately involved in regulating the nuclear translocation of NPRL2 in response to RT.

We hypothesize that the dissociation of WDR24 from the GATOR2 complex is critical for NPRL2 to exert its functional role. Reports indicate that WDR24 dissociation is regulated by AMPK activation, which phosphorylates WDR24, promoting its separation[15]. Thus, we asked whether RT regulates the spatio-temporal distribution of NPRL2 *via* the AMPK/WDR24 axis, and sought to investigate this systematically. As a starting point, we observed that RT effectively induces AMPK activation in a time-dependent manner (Fig. 4C). However, whether RT-triggered AMPK activation facilitates WDR24 dissociation from the GATOR2 complex remains uncertain. Our Co-IP analysis demonstrated that after RT, the interaction between WDR24 and WDR59/SEC13 was significantly reduced. Crucially, this reduction in interaction can be fully reversed by a specific AMPK inhibitor (Dorsomorphin) (Fig. 4D). This underscores that RT can indeed prompt WDR24 dissociation through AMPK activation, and inhibiting AMPK activation can maintain WDR24 within the GATOR2 complex (Fig. 4E). Subsequently, we examined the impact of WDR24 dissociation on subsequent processes. Through Co-IP experiments, we discovered that 6 h post-RT, WDR24 associates with two GATOR1 members, NPRL2 and DEPDC5. Concurrently, the original NPRL2−DEPDC5 interaction disintegrated. Notably, the binding between WDR24 and another GATOR2 constituent, SEH1L, also significantly diminished upon initiation of RT, suggesting that RT promoted the dissociation of WDR24 from the complex (Fig. 4F). Temporal analysis further revealed that over 0−6 h of RT, the association between NPRL2 and DEPDC5 gradually weakened, while the binding between WDR24 and NPRL2 concurrently strengthened (Fig. 4G). These processes suggest that RT induces WDR24 dissociation, enabling its integration into the GATOR1 complex, which leads to the complete dissociation of NPRL2 from GATOR1. However, these processes were impeded by AMPK inhibition; the inhibitor retained WDR24 within the GATOR2 complex following RT, thereby preventing the spatial and temporal release of NPRL2 (Fig. 4E and F), as confirmed by nuclear-cytoplasmic separation experiments (Fig. 4H). To further validate the mechanistic link between AMPK activation and NPRL2 nuclear accumulation, we generated AMPKα-KO CRC models. Notably, the loss of AMPKα completely abolished radiation-induced AMPK phosphorylation, confirming the successful disruption of AMPK signaling. Importantly, NPRL2 nuclear translocation was robustly induced by radiation in control cells, which was entirely blocked in AMPKα-KO models (Fig. 4I). In summary, RT-induced NPRL2 dissociation from GATOR1 and its subsequent nuclear translocation depend on the AMPK/WDR24 axis. Inhibition or knockout of AMPK retains NPRL2 within GATOR1, thereby preventing its nuclear translocation (Fig. 4J).

IHC analysis of clinical specimens demonstrated that while total AMPK levels remained unchanged following radiotherapy and showed no association with NPRL2 nuclear localization (Supporting Information Fig. S8A), p-AMPK was significantly upregulated in tumor cells post-RT (Fig. S8B and S8C), consistent with our *in vitro* findings. Although p-AMPK levels did not demonstrate a definitive correlate with patient survival outcomes (Fig. S8D and S8E), they exhibited a strong post-RT specific association with NPRL2 nuclear accumulation (Fig. 4K), providing direct clinical evidence that radiation-induced AMPK activation drives NPRL2 nuclear translocation in CRC patients.

3.5. AMPK inhibition impairs DNA repair by preventing NPRL2 nuclear translocation, thereby sensitizing CRC cells to RT

Inhibiting AMPK activation hinders the nuclear translocation of NPRL2, thereby impacting its interaction with E3 ligases such as HERC2 or RNF8, though the precise nature of this effect remains unclear. To further elucidate this, initial Co-IP experiments demonstrated that treatment with the AMPK inhibitor Dorsomorphin markedly inhibited the interactions between NPRL2 and

2 h post-irradiation. Nuclear (N) and cytoplasmic (C) fractions were separated and analyzed. WCL WB analysis for knockout effect (Right). (B-D, F-I), all WB or Co-IP analyses were replicated in triplicate. (J) Schematic illustration for the AMPK−GATOR1 signaling pathway in CRC cells treated with Dorsomorphin (10 μmol/L) following 6 Gy IR: After radiotherapy, NPRL2 dissociates from the GATOR1 complex and translocates from the cytoplasm to the nucleus. This process depends on the AMPK/WDR24 axis. AMPK inhibitors can retain NPRL2 in the GATOR1 complex, preventing its nuclear translocation. (K) Spearman's correlation between nuclear p-AMPK and NPRL2 levels in the (K-1) SYSUCC cohort and (K-2) SYSUFAH cohort pre- and post-CRT. The number of samples for this figure is annotated on each image.

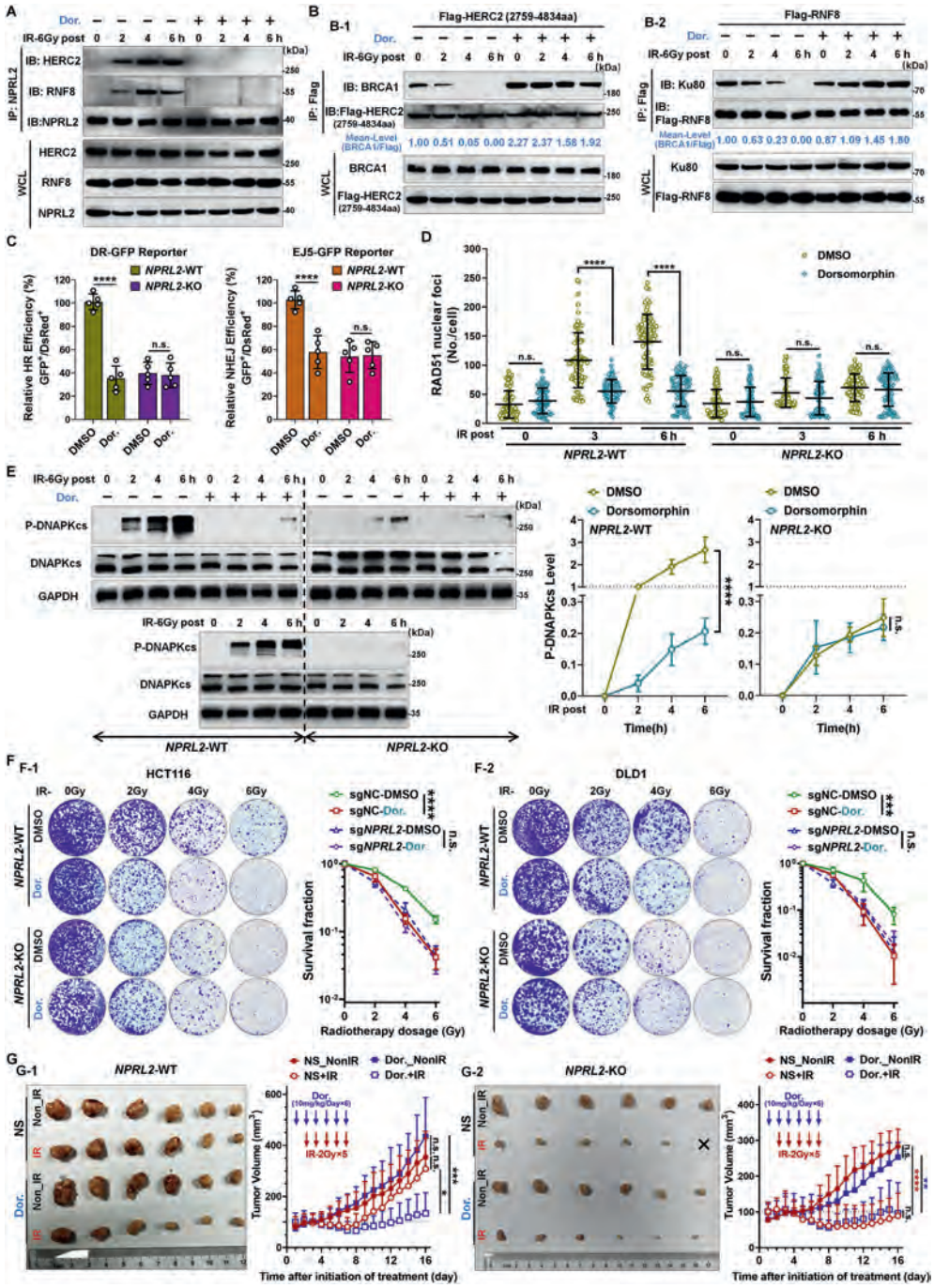

Figure 5 AMPK inhibition impairs DNA repair by preventing NPRL2 nuclear translocation, thereby sensitizing CRC cells to RT. (A) Co-IP and WB analysis of the interaction between NPRL2 and HERC2, RNF8 in HCT116 cells treated with Dorsomorphin (10 μmol/L) for 3 h and then exposed to 6 Gy IR. Cells were collected at specific time points (0, 2, 4, and 6 h) after IR. (B) Co-IP and WB assays detecting the interaction between (B-1) Flag-HERC2 (2759−4834aa) and BRCA1 (B-2) Flag-RNF8 and Ku80 in HCT116 cells treated with Dorsomorphin (10 μmol/L) for 3 h and then exposed to 6 Gy IR. Cells were collected at specific time points (0, 2, 4, and 6 h) after IR. The mean levels of BRCA1, normalized to Flag-HERC2, and Ku80, normalized to Flag-RNF8, are shown below each lane. (A, B) All WB analysis or Co-IP analysis were replicated in triplicate. (C) The HR and NHEJ reporter assays for the analysis of DNA DSB repair pathways in NPRL2-WT or -KO HCT116 cells treated with Dorsomorphin (10 μmol/L) for 3 h and then exposed to 6 Gy IR. Cells were collected at 24 h after IR. Successful repair restores GFP expression, which was quantified by flow cytometry. All statistical data are presented as mean ± SD ($n = 5$; two-way ANOVA), $^{****}P < 0.0001$; n.s., not significant. (D) IF images depicting the RAD51 nuclear foci in HCT116 cells (NPRL2-WT and NPRL2-KO) after 6 Gy IR, pretreated with Dorsomorphin (Dor., 10 μmol/L) or DMSO (as a control) for 3 h. Cells were fixed at the indicated time points (0, 3, 6 h) post-IR and stained for RAD51 (green) and nuclei (blue). Quantifies RAD51 nuclear foci per cell under each condition. Data are presented as mean ± SD (two-way ANOVA), $^{****}P < 0.0001$; n.s., not significant. (E) WB assays detecting the *p*-DNA-PKcs and DNA-PKcs levels in HCT116 cells (NPRL2-WT and NPRL2-KO) after 6 Gy IR, pretreated with Dorsomorphin (Dor., 10 μmol/L) or DMSO (as a control) for 3 h. Cells are collected at specific

HERC2 (Fig. 5A), as well as NPRL2 and RNF8 (Fig. 5B). Consequently, the disruption of these interactions abrogates NPRL2's capacity to sequester and regulate HERC2 and RNF8, thereby promoting direct binding of HERC2 to BRCA1 and RNF8 to Ku80 (Fig. 5A and B). These findings are consistent with observations following NPRL2 knockout, providing additional mechanistic insights into the function of NPRL2. Subsequent assays assessing DNA repair efficacy revealed that Dorsomorphin significantly reduced HR and NHEJ activities, but only when NPRL2 was present. Following NPRL2 knockout, Dorsomorphin no longer exerted additional inhibitory effects on HR or NHEJ repair, with its impact resembling that of NPRL2 knockout alone (Fig. 5C and Supporting Information Fig. S9). These findings, observed consistently in two distinct CRC cell lines, underscore that AMPK inhibition impedes the NPRL2 nuclear translocation-mediated enhancement of DNA repair efficiency.

To further validate the influence of NPRL2 nuclear translocation on HR or NHEJ repair dynamics, we assessed representative markers specific to each pathway. In HR repair, nuclear localization of RAD51 recombinase serves as a pivotal indicator of repair proficiency. We quantified RAD51 nuclear foci to evaluate this process, revealing that in the presence of NPRL2, RAD51 foci exhibited a time-dependent increase post-RT (0−6 h). However, treatment with Dorsomorphin markedly attenuated this increase, resulting in only a marginal, statistically non-significant rise relative to baseline (Fig. 5D and Supporting Information Fig. S10). These findings indicate that Dorsomorphin effectively impedes RAD51 recruitment, thereby suppressing HR repair. Importantly, NPRL2 knockout produced similar effects, significantly reducing RAD51 nuclear foci formation post-RT. This effect parallels AMPK inhibition, with Dorsomorphin producing no additional impact (Fig. 5D and Fig. S10). These results indicate that AMPK inhibitors hinder HR repair by restricting the NPRL2 nuclear translocation process. In NHEJ repair, the auto-activation of core factor DNA-PKcs is essential for recruiting and activating downstream repair factors or the synapse complex. Thus, we evaluated the activation state of DNA-PKcs to discern its broader implications for the NHEJ pathway. Our findings revealed that, in the presence of NPRL2, Dorsomorphin disrupted the post-RT increase in DNA-PKcs phosphorylation levels. This inhibition of DNA-PKcs activation was notably pronounced compared to conditions without Dorsomorphin and closely resembled the effects observed following NPRL2 knockout. Similarly, Dorsomorphin did not exert any additional inhibitory effect in NPRL2-deficient cells (Fig. 5E). These findings suggest that AMPK inhibitors suppress NHEJ repair by similarly impeding the NPRL2 nuclear translocation.

Finally, to further validate functional outcomes, we conducted colony formation assays to evaluate the impact of radiotherapy on the survival capacity of CRC cells. The results demonstrated that the presence of NPRL2 significantly enhanced the radiosensitizing effect of Dorsomorphin. Conversely, NPRL2 knockout increased the sensitivity of CRC cells to radiotherapy to a level comparable to the synergistic effect of Dorsomorphin in NPRL2-proficient cells. Notably, Dorsomorphin did not further enhance this synergistic effect in NPRL2-deficient cells. These functional outcomes were consistently reproduced in two distinct CRC cell lines (Fig. 5F). Additionally, Dorsomorphin, an AMPK inhibitor, partially restored radiosensitivity in radioresistant HCT116 cells, particularly at higher radiation doses (>6 Gy). While NPRL2 knockout significantly reversed radioresistance, the addition of Dorsomorphin provided no further increase in radiosensitivity, indicating that NPRL2 nuclear translocation is essential for AMPK-mediated radioresistance (Supporting Information Fig. S11). To further delineate the causal role of NPRL2 in radioresistance, we performed complementary loss-of-function experiments *in vivo*. NPRL2-knockout tumors exhibited markedly improved radiation sensitivity. AMPK inhibition with Dorsomorphin phenocopied this radiosensitization effect by blocking NPRL2 nuclear translocation. Crucially, Dorsomorphin lost its efficacy in NPRL2-KO models, confirming that its action specifically depends on modulating NPRL2 localization (Fig. 5G and Supporting Information Fig. S12). In conclusion, the synergistic effects mediated by AMPK inhibitors depend on the presence of NPRL2, underscoring the therapeutic potential of NPRL2 nuclear translocation. Altogether, our targeting strategy and functional analyses demonstrate the potential of targeting AMPK to inhibit NPRL2 nuclear translocation, thereby enhancing radiosensitivity in CRC therapy.

4. Discussion

HR is a high-fidelity DNA repair mechanism that relies on a homologous DNA template and is primarily active during the S and G2 phases of the cell cycle. In contrast, NHEJ is a more error-prone process that functions throughout the cell cycle and does not require a homologous template. The choice between HR and NHEJ is determined by the cell cycle stage, the extent of DNA end resection, and the availability of specific repair proteins[5]. These two pathways frequently compete for access to DNA double-strand breaks. For instance, DNA end resection is a key step that promotes HR by generating the single-stranded DNA necessary for its machinery. However, when DNA end resection is inhibited, NHEJ is more likely to prevail. Proteins such as 53BP1 and BRCA regulate this competition, with 53BP1 promoting NHEJ and BRCA1 facilitating HR[26,27]. The initiation and progression of these two repair mechanisms largely determine the fate of tumor cells following radiotherapy. Consequently, research into the regulation of HR and NHEJ continues to advance, aiming to elucidate the underlying mechanisms of radiotherapy resistance.

Ubiquitination plays a crucial role in regulating various cellular processes, including alterations in the tumor microenvironment, DNA damage response, and cell cycle regulation, all of which are pivotal in determining the sensitivity of cancer cells

time points (0, 2, 4, and 6 h) after IR. Left: representative images. Right: relative *p*-DNA-PKcs levels, presented as the ratio of P-DNA-PKcs to GAPDH grayscale values at the indicated time points, normalized to the 0 h level. Data are presented as mean ± SD (two-way ANOVA), $****P < 0.0001$; n.s., not significant. (F) Colony formation assays in (F-1) HCT116 and (F-2) DLD1 cells treated with Dorsomorphin (10 μmol/L) for 3 h and subsequently with a single dose of 0, 2, 4, 6 Gy IR. Left, representative images. Right, survival fraction, shown as mean ± SD from 3 independent experiments (two-way ANOVA, DMSO as a control, $****P < 0.0001$; $***P < 0.001$; n.s., not significant). (G) NPRL2-WT and NPRL2-KO HCT116 xenografts were treated alternately with Dorsomorphin (10 mg/kg/day for 5 times, normal saline (NS) as control) and IR (2-Gy/day for 5 times). Representative images of tumors (G-1) and quantitative analysis of tumor volume (G-2). Data are mean ± SD ($n = 6$/group). Statistical significance was determined by two-way ANOVA (n.s., not significant; $*P < 0.05$, $**P < 0.01$, $***P < 0.001$, $****P < 0.0001$).

to radiotherapy[28]. E3 ubiquitin ligases regulate cancer cell DNA damage repair by targeting specific substrates for ubiquitin-mediated degradation[29]. HUWE1, a HECT-type E3 ligase, plays a crucial role in DNA repair and cancer progression[29-31]. It regulates DNA damage repair by ubiquitinating and promoting the degradation of proteins such as H2AX and BRCA1, both of which are essential for HR[32]. RNF138 is crucial for DNA damage repair by binding to damage sites *via* its zinc finger domain and ubiquitinating key repair factors, including RAD51, which influences HR-mediated repair[29,33]. The RING-type E3 ligases RNF126 and BRCA2 are crucial in DNA damage repair and cancer development, with RNF126 specifically targeting Ku80 for polyubiquitination, facilitating the dissociation of Ku70/Ku80 from DNA, and accelerating non-homologous end joining (NHEJ)-mediated repair in cells[29,34]. RNF8 and RNF168 ubiquitinate histones, thereby creating a platform for the recruitment of repair proteins such as 53BP1 and BRCA1, and promoting effective DNA repair[35]. RNF8 regulates the levels of the NHEJ repair protein Ku80 at DNA damage sites, and its depletion leads to the prolonged retention of Ku80 at these sites, ultimately impairing the efficiency of NHEJ repair[11,36]. In our study, we observed that nuclear K48-linked ubiquitination levels correlate with the efficacy of radiotherapy. Following extensive validation, we also directed our attention to the impact of E3 ligase regulation on DNA repair and radioresistance. This focus represents a preliminary step toward investigating novel regulatory mechanisms.

Building on the approach as mentioned above, we have identified NPRL2 as an important factor in radiotherapy resistance. Upon exposure to radiotherapy signals, NPRL2 translocates to the nucleus, where it exploits its distinct structural characteristics to bind and occupy the ubiquitin-binding regions or ubiquitin-transfer domains of specific nuclear E3 ligases, thereby impeding their enzymatic functions. Notably, these E3 ligases are critical regulators of the HR or NHEJ pathways, including RNF8, HERC2, and HUWE1. That said, E3 ligases are responsible for tagging these targets with ubiquitin, marking them for degradation by the proteasome. This process is essential for the timely removal and recycling of DNA repair factors, ensuring their presence only when needed and preventing inappropriate or prolonged activation of repair pathways. Inhibition of E3 ligases, including RNF168, RNF8, MDM2, and HUWE1 as mentioned above, impairs DNA repair processes, increases DNA damage, and promotes genomic instability[29,30,37-39].

In this article, we have uncovered common regulatory mechanisms involving E3 ligases that operate upstream in the DNA damage repair process. Following radiotherapy, NPRL2 translocates from the cytoplasm to the nucleus, where it interacts with

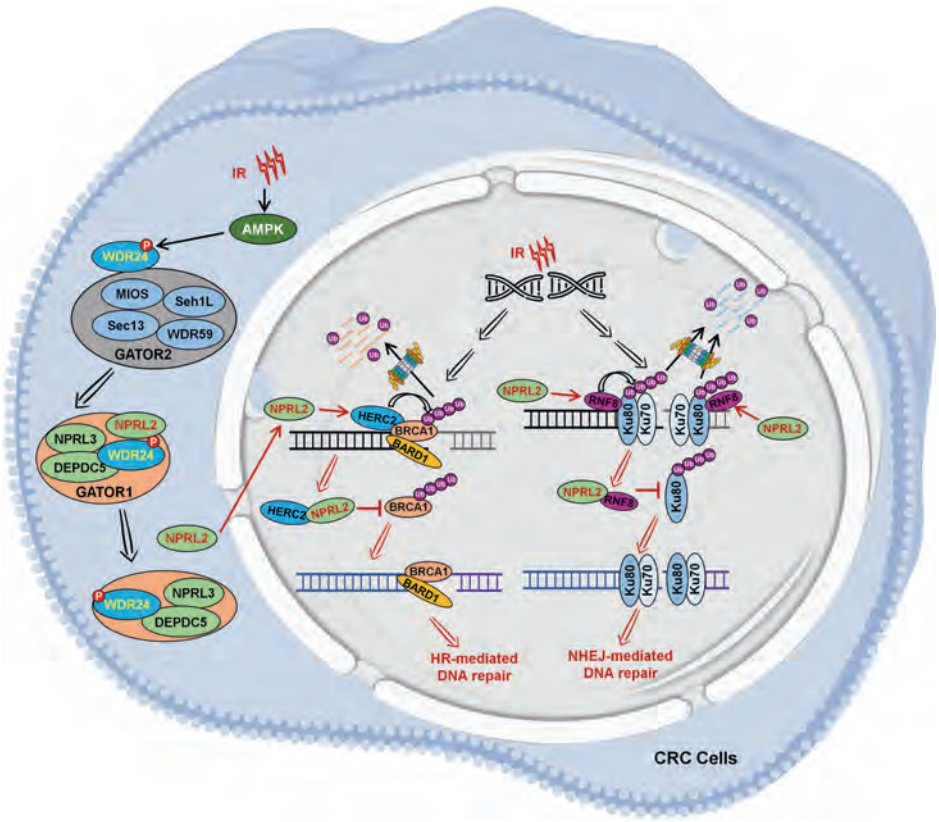

Figure 6 The AMPK−WDR24−NPRL2 signaling pathway and its involvement in DNA repair processes following RT. Upon IR exposure, AMPK is activated and phosphorylates WDR24, leading to its dissociation from the GATOR2 complex (composed of MIOS, Sec13, WDR59, and SEH1L). This promotes the association of WDR24 with the GATOR1 complex (NPRL2, DEPDC5, NPRL3), facilitating the nuclear translocation of NPRL2. Once in the nucleus, NPRL2 interacts with E3 ubiquitin ligases such as HERC2 and RNF8. These interactions inhibit the ubiquitination activity of HERC2 and RNF8, particularly affecting proteins involved in the HR-mediated DNA repair (*e.g.*, BRCA1−BARD1) and NHEJ-mediated DNA repair (*e.g.*, Ku70−Ku80). This disruption of E3 ligase activity supports the preservation of DNA damage repair homeostasis, contributing to radiotherapy resistance in CRC cells.

specific domains of nuclear K48-linked E3 ligases—key regulators of DNA damage repair factors. Once within the nucleus, NPRL2 hijacks the E3 ligases, preventing the degradation of DNA repair factors and ensuring their continuous involvement in the repair process, thereby sustaining the progression of both NHEJ and HR pathways. Consequently, targeting the nuclear translocation of NPRL2 may effectively inhibit DNA damage repair mediated by NHEJ and HR, thereby sensitizing cells to radiotherapy. Our observations indicate that the selective sequestration of E3 ligases by NPRL2 upon nuclear entry significantly enhances the HR and NHEJ repair pathways, thereby facilitating the continuous progression of DNA repair mechanisms. We hypothesize that this phenomenon is directly associated with the extent of DNA damage caused by radiation. Notably, after fulfilling their initial roles, repair proteins are not degraded by the proteasome; instead, they are redeployed to subsequent damage sites, sustaining reparative functions. This deviation from the conventional paradigm of protein turnover regulation significantly enhances DNA repair efficiency and confers a marked advantage in mitigating radiation-induced damage.

We remain intrigued by the mechanisms through which NPRL2 selectively targets E3 ligases. Protein docking analyses and *in vitro* validations demonstrated that NPRL2 binds to the HERT domain of HERC2, the HECT domain of HUWE1, and the RING (really interesting new gene) domain of RNF8. However, after translocating into the nucleus, NPRL2 fails to associate with either RNF168 or TRIM21, indicating that this phenomenon may be attributed to the structural properties of E3 ligases. Historically, E3 ligases were categorized based on domain types related to ubiquitination processes, specifically the RING and HECT domains[25,40-43]. However, with the advancement of research, it has become clear that E3 ligases can also be differentiated by the nature of the substrates they modify or by their ubiquitination patterns. In this context, we undertook a detailed examination of the structural attributes of RNF168 and TRIM21[44-47], discovering that their ubiquitin-related domains do not conform to the RING or HECT classifications, which likely accounts for the lack of interaction between NPRL2 and these proteins. Nonetheless, the extent to which NPRL2 depends on these structural characteristics to selectively bind ligases warrants further comprehensive investigation, representing a critical focal point for subsequent research efforts.

Additionally, this study investigates the mechanism by which radiotherapy induces the nuclear entry of NPRL2, and highlights the essential role of WDR24, a key component of the GATOR2 complex, in this process. The activation of WDR24 is necessary for both its release from the GATOR2 complex and its interaction with the GATOR1 complex, thereby facilitating the release of NPRL2 (Fig. 6).

Previous studies have established that AMPK plays a critical role in the cellular response to radiotherapy, contributing to radioresistance by regulating the cell cycle and DNA damage repair *via* NHEJ[18,48]. Here, we uncover a novel mechanism by which AMPK activates WDR24 to promote NPRL2 nuclear translocation, ultimately leading to resistance to radiotherapy. In other words, AMPK, as an upstream sensor molecule after radiotherapy, may contribute to radioresistance through multiple pathways.

Subsequent experiments confirmed that inhibiting AMPK activity effectively trapped NPRL2 within the GATOR1 complex, preventing NPRL2 nuclear translocation, blocking subsequent DNA repair, and ultimately enhancing radiosensitivity. Elucidating the key mechanism by which the AMPK/WDR24/NPRL2 signaling axis offers a potential target for the development of future radiosensitizing therapies.

5. Conclusions

The AMPK—WDR24—NPRL2 signaling pathway and its role in DNA repair processes following IR. Upon IR exposure, AMPK is activated and phosphorylates WDR24, triggering its dissociation from the GATOR2 complex (composed of MIOS, SEC13, WDR59, and SEH1L). This promotes the association of WDR24 with the GATOR1 complex (NPRL2, DEPDC5, NPRL3), facilitating the translocation of NPRL2 to the nucleus. Once in the nucleus, NPRL2 interacts with E3 ubiquitin ligases such as HERC2 and RNF8. These interactions inhibit the ubiquitination activity of HERC2 and RNF8, particularly affecting proteins involved in the HR-mediated DNA repair (*e.g.*, BRCA1—BARD1) and NHEJ-mediated DNA repair (*e.g.*, Ku70—Ku80). This disruption of E3 ligase activity supports the preservation of DNA damage repair homeostasis, contributing to resistance to radiotherapy in CRC cells.

Ethics declarations

Informed consent was obtained from all participants in the study. Accordingly, all methods involving primary human samples were performed in accordance with the relevant guidelines and regulations and were approved by Institutional Ethics Committee for Clinical Research and Animal Trials of The First Affiliated Hospital, Sun Yat-sen University (SYSUFAH) (Ethical Approval No. is [2023]079); The Institutional Ethical Boards of Sun Yat-sen University Cancer Center (SYSUCC) (Ethical Approval No. is 202310024).

Acknowledgments

This project was supported by the National Natural Science Foundation of China (NSFC) (No. 82373209 to Xuecen Wang; 82272743 to Xin Yue; 82373203 to Yong Chen and 82373379 to Ran-yi Liu), Funding by Science and Technology Projects in Guangzhou (No. 2024A04J4633 to Xuecen Wang and 2025A04J0177 to Xin Yue, China) from the Science and Technology Projects of Guangzhou, the Kelin Rising Star Talent Program from The First Affiliated Hospital (No. R08039 to Xuecen Wang, China), and the Basic Scientific Research Operation of Sun Yat-sen University (No. 24qnpy335 to Xuecen Wang, China).

Author contributions

Study concept and design: Xin Yue, Yong Bao and Ran-yi Liu; Performed *in vitro* functional studies and analyzed data: Xuecen Wang, Yuxuan Zhao, Xingli Yang and Tingyu Liu; Generated critical cellular tools: Xuecen Wang, Xingli Yang and Tingyu Liu.; Performed mechanistical studies and analyzed data: Xin Yue, Xuecen Wang, Yuxuan Zhao; Collection and organization of clinical data: Xuecen Wang and Shaoqing Niu; Statistical analysis: Meng Jin and Xuecen Wang; Supervision of data: Yong Bao and Yong Chen; Analysis and interpretation of data and writing of the

manuscript: Xuecen Wang and Xin Yue. All authors have read and approved the manuscript.

Conflicts of interest

None of the authors have any potential conflicts to disclose.

Appendix A. Supporting information

Supporting information to this article can be found online at https://doi.org/10.1016/j.apsb.2025.10.039.

References

1. Sung H, Ferlay J, Siegel RL, Laversanne M, Soerjomataram I, Jemal A, et al. Global cancer statistics 2020: GLOBOCAN estimates of incidence and mortality worldwide for 36 cancers in 185 countries. *CA Cancer J Clin* 2021;**71**:209−49.
2. Häfner MF, Debus J. Radiotherapy for colorectal cancer: current standards and future perspectives. *Visc Med* 2016;**32**:172−7.
3. Jackson SP, Bartek J. The DNA-damage response in human biology and disease. *Nature* 2009;**461**:1071−8.
4. Tan J, Sun X, Zhao H, Guan H, Gao S, Zhou PK. Double-strand DNA break repair: molecular mechanisms and therapeutic targets. *MedComm* 2023;**4**:e388.
5. Ceccaldi R, Rondinelli B, D'Andrea AD. Repair pathway choices and consequences at the double-strand break. *Trends Cell Biol* 2016;**26**: 52−64.
6. Hoeller D, Hecker C-M, Dikic I. Ubiquitin and ubiquitin-like proteins in cancer pathogenesis. *Nat Rev Cancer* 2006;**6**:776−88.
7. Chen Q, Zheng W, Guan J, Liu H, Dan Y, Zhu L, et al. SOCS2-enhanced ubiquitination of SLC7A11 promotes ferroptosis and radiosensitization in hepatocellular carcinoma. *Cell Death Differ* 2023;**30**: 137−51.
8. Wang X, Cao Z, Yue X, Liu T, Wen G, Jiang D, et al. Stabilization of DEPTOR sensitizes hypopharyngeal cancer to radiotherapy *via* targeting degradation. *Mol Ther Oncolytics* 2022;**26**:330−46.
9. Grabbe C, Husnjak K, Dikic I. The spatial and temporal organization of ubiquitin networks. *Nat Rev Mol Cell Biol* 2011;**12**: 295−307.
10. Yue X, Liu T, Wang X, Wu W, Wen G, Yi Y, et al. Pharmacological inhibition of BAP1 recruits HERC2 to competitively dissociate BRCA1-BARD1, suppresses DNA repair and sensitizes CRC to radiotherapy. *Acta Pharm Sin B* 2023;**13**:3382−99.
11. Bekker-Jensen S, Rendtlew Danielsen J, Fugger K, Gromova I, Nerstedt A, Lukas C, et al. HERC2 coordinates ubiquitin-dependent assembly of DNA repair factors on damaged chromosomes. *Nat Cell Biol* 2010;**12**:80−6.
12. Guo Z, Wang S, Xie Y, Han Y, Hu S, Guan H, et al. HUWE1-dependent DNA-PKcs neddylation modulates its autophosphorylation in DNA damage response. *Cell Death Dis* 2020; **11**:400.
13. Bar-Peled L, Chantranupong L, Cherniack AD, Chen WW, Ottina KA, Grabiner BC, et al. A tumor suppressor complex with GAP activity for the Rag GTPases that signal amino acid sufficiency to mTORC1. *Science* 2013;**340**:1100−6.
14. Sadria M, Seo D, Layton AT. The mixed blessing of AMPK signaling in cancer treatments. *BMC Cancer* 2022;**22**:105.
15. Dai X, Jiang C, Jiang Q, Fang L, Yu H, Guo J, et al. AMPK-dependent phosphorylation of the GATOR2 component WDR24 suppresses glucose-mediated mTORC1 activation. *Nat Metab* 2023; **5**:265−76.
16. Valenstein ML, Rogala KB, Lalgudi PV, Brignole EJ, Gu X, Saxton RA, et al. Structure of the nutrient-sensing hub GATOR2. *Nature* 2022;**607**:610−6.
17. Jin H, Gao S, Guo H, Ren S, Ji F, Liu Z, et al. Re-sensitization of radiation resistant colorectal cancer cells to radiation through inhibition of AMPK pathway. *Oncol Lett* 2016;**11**:3197−201.
18. Sanli T, Rashid A, Liu C, Harding S, Bristow RG, Cutz JC, et al. Ionizing radiation activates AMP-activated kinase (AMPK): a target for radiosensitization of human cancer cells. *Int J Radiat Oncol Biol Phys* 2010;**78**:221−9.
19. Jiang Y, Dong Y, Luo Y, Jiang S, Meng FL, Tan M, et al. AMPK-mediated phosphorylation on 53BP1 promotes c-NHEJ. *Cell Rep* 2021;**34**:108713.
20. Tong Y, Liu D, Zhang J. Connection and distinction of tumor regression grading systems of gastrointestinal cancer. *Pathol Res Pract* 2020;**216**: 153073.
21. Wang XC, Yue X, Zhang RX, Liu TY, Pan ZZ, Yang MJ, et al. Genome-wide RNAi screening identifies RFC4 as a factor that mediates radioresistance in colorectal cancer by facilitating nonhomologous end joining repair. *Clin Cancer Res* 2019;**25**: 4567−79.
22. Liu F, Chen J, Li K, Li H, Zhu Y, Zhai Y, et al. Ubiquitination and deubiquitination in cancer: from mechanisms to novel therapeutic approaches. *Mol Cancer* 2024;**23**:148.
23. Popovic D, Vucic D, Dikic I. Ubiquitination in disease pathogenesis and treatment. *Nat Med* 2014;**20**:1242−53.
24. van Wijk SJ, Fulda S, Dikic I, Heilemann M. Visualizing ubiquitination in mammalian cells. *EMBO Rep* 2019;**20**:e46520.
25. Zheng N, Shabek N. Ubiquitin ligases: structure, function, and regulation. *Annu Rev Biochem* 2017;**86**:129−57.
26. Scully R, Panday A, Elango R, Willis NA. DNA double-strand break repair-pathway choice in somatic mammalian cells. *Nat Rev Mol Cell Biol* 2019;**20**:698−714.
27. Symington LS, Gautier J. Double-strand break end resection and repair pathway choice. *Annu Rev Genet* 2011;**45**:247−71.
28. Zhang M, Shao Y, Gu W. The mechanism of ubiquitination or deubiquitination modifications in regulating solid tumor radiosensitivity. *Biomedicines* 2023;**11**:3240.
29. Yang Q, Zhao J, Chen D, Wang Y. E3 ubiquitin ligases: styles, structures and functions. *Mol Biomed* 2021;**2**:23.
30. Senft D, Qi J, Ronai ZeA. Ubiquitin ligases in oncogenic transformation and cancer therapy. *Nat Rev Cancer* 2018;**18**:69−88.
31. Kao SH, Wu HT, Wu KJ. Ubiquitination by HUWE1 in tumorigenesis and beyond. *J Biomed Sci* 2018;**25**:67.
32. Wang X, Lu G, Li L, Yi J, Yan K, Wang Y, et al. HUWE1 interacts with BRCA1 and promotes its degradation in the ubiquitin−proteasome pathway. *Biochem Biophys Res Commun* 2014; **444**:290−5.
33. Yard BD, Reilly NM, Bedenbaugh MK, Pittman DL. RNF138 interacts with RAD51D and is required for DNA interstrand crosslink repair and maintaining chromosome integrity. *DNA Repair* 2016;**42**: 82−93.
34. Ishida N, Nakagawa T, Iemura S-I, Yasui A, Shima H, Katoh Y, et al. Ubiquitylation of Ku80 by RNF126 promotes completion of nonhomologous end joining-mediated DNA repair. *Mol Cell Biol* 2017;**37**: e00347.
35. Mallette FA, Mattiroli F, Cui G, Young LC, Hendzel MJ, Mer G, et al. RNF8- and RNF168-dependent degradation of KDM4A/JMJD2A triggers 53BP1 recruitment to DNA damage sites. *EMBO J* 2012;**31**: 1865−78.
36. Feng L, Chen J. The E3 ligase RNF8 regulates KU80 removal and NHEJ repair. *Nat Struct Mol Biol* 2012;**19**:201−6.
37. Sato K, Sundaramoorthy E, Rajendra E, Hattori H, Jeyasekharan AD, Ayoub N, et al. A DNA-damage selective role for BRCA1 E3 ligase in claspin ubiquitylation, CHK1 activation, and DNA repair. *Curr Biol* 2012;**22**:1659−66.
38. Hu Q, Botuyan MV, Zhao D, Cui G, Mer E, Mer G. Mechanisms of BRCA1−BARD1 nucleosome recognition and ubiquitylation. *Nature* 2021;**596**:438−43.
39. Liu W, Zheng M, Zhang R, Jiang Q, Du G, Wu Y, et al. RNF126-mediated MRE11 ubiquitination activates the DNA damage response

and confers resistance of triple-negative breast cancer to radiotherapy. *Adv Sci* 2023;**10**:e2203884.
40. Deshaies RJ, Joazeiro CAP. RING domain E3 ubiquitin ligases. *Annu Rev Biochem* 2009;**78**:399−434.
41. Lechtenberg BC, Rajput A, Sanishvili R, Dobaczewska MK, Ware CF, Mace PD, et al. Structure of a HOIP/E2∼ubiquitin complex reveals RBR E3 ligase mechanism and regulation. *Nature* 2016;**529**:546−50.
42. Petroski MD, Deshaies RJ. Function and regulation of cullin−RING ubiquitin ligases. *Nat Rev Mol Cell Biol* 2005;**6**:9−20.
43. Buetow L, Huang DT. Structural insights into the catalysis and regulation of E3 ubiquitin ligases. *Nat Rev Mol Cell Biol* 2016;**17**: 626−42.
44. Wu W, Zhao Y, Qin B, Jiang X, Wang C, Hu R, et al. Non-canonical role of UCKL1 on ferroptosis defence in colorectal cancer. *EBioMed* 2023;**93**:104650.
45. Mukadam AS, Miller LVC, Smith AE, Vaysburd M, Sakya SA, Sanford S, et al. Cytosolic antibody receptor TRIM21 is required for effective tau immunotherapy in mouse models. *Science (New York, NY)* 2023;**379**:1336−41.
46. Mattiroli F, Vissers JHA, van Dijk WJ, Ikpa P, Citterio E, Vermeulen W, et al. RNF168 ubiquitinates K13−15 on H2A/H2AX to drive DNA damage signaling. *Cell* 2012;**150**: 1182−95.
47. Stewart GS, Panier S, Townsend K, Al-Hakim AK, Kolas NK, Miller ES, et al. The RIDDLE syndrome protein mediates a ubiquitin-dependent signaling cascade at sites of DNA damage. *Cell* 2009;**136**: 420−34.
48. Zannella VE, Cojocari D, Hilgendorf S, Vellanki RN, Chung S, Wouters BG, et al. AMPK regulates metabolism and survival in response to ionizing radiation. *Radiother Oncol* 2011;**99**:293−9.